Taylor's hypothesis in turbulent channel flow considered using a transport equation analysis

Chenhui Geng, Guowei He, Yinshan Wang, Chunxiao Xu, Adrián Lozano-Durán, and James M. Wallace

Articles you may be interested in

Computational study of flow-induced vibration of a reed in a channel and effect on convective heat transfer
Phys. Fluids 26, 127103 (2014); 10.1063/1.4903793

Drag reduction effect by a wave-like wall-normal body force in a turbulent channel flow
Phys. Fluids 26, 115104 (2014); 10.1063/1.4901186

Turbulence and skin friction modification in channel flow with streamwise-aligned superhydrophobic surface texture
Phys. Fluids 26, 095102 (2014); 10.1063/1.4894064

Exact transport equation for local eddy viscosity in turbulent shear flow
Phys. Fluids 25, 085102 (2013); 10.1063/1.4816702

Direction of scalar transport in turbulent channel flow
Phys. Fluids 23, 115105 (2011); 10.1063/1.3657825

Taylor's hypothesis in turbulent channel flow considered using a transport equation analysis

Chenhui Geng, Guowei He, Yinshan Wang,[a] Chunxiao Xu,[a]
Adrián Lozano-Durán,[b] and James M. Wallace[c]
*State Key Laboratory of Nonlinear Mechanics, Institute of Mechanics, Chinese Academy of
Sciences, Beijing 100190, China*

Direct numerical simulations of turbulent channel flow at $Re_\tau = 205$ and 932 have
been carried out to examine Taylor's "frozen turbulence" hypothesis. The terms in
Taylor's hypothesis appear in the transport equation for instantaneous momentum
(Navier-Stokes) in this flow. The additional terms, i.e., the additional convective
acceleration term and the pressure gradient and viscous force terms, act to diminish
the validity of Taylor's hypothesis when they are relatively large compared to the
Taylor's hypothesis terms and are not in balance. A similar analysis has been
applied to the transport equation for instantaneous vorticity. The additional terms
in this equation, namely, the additional convective rates of change of vorticity terms,
the stretching/compression/rotation of vorticity terms, and the viscous diffusion of
vorticity terms, similarly act to diminish the validity of Taylor's hypothesis when
they are relatively large compared to the terms in the hypothesis and are not in
balance. Where in the channel flow this diminishment occurs, and to what degree, and
which of the non-Taylor's hypothesis terms in the momentum and vorticity equations
contribute most to this diminishment are unraveled here. © *2015 AIP Publishing
LLC.* [http://dx.doi.org/10.1063/1.4908070]

I. INTRODUCTION

Taylor,[1] in his paper, on the production and dissipation of vorticity in turbulence, first suggested
the idea that became known as his hypothesis. The idea is that streamwise derivatives $\partial/\partial x$ of ve-
locity fluctuations in turbulent flows can be approximated by $(1/\overline{U})\partial/\partial t$, i.e., by a simple time-space
derivative transformation, where x is the streamwise direction of the mean velocity, $\overline{U}$, and t is time.
Taylor[2] submitted a paper two months later on ". . . the connexion between the spectrum of turbulence,
measured at a fixed point, and the correlation between *simultaneous* [his emphasis] values of velocity
measured at two points." There he qualified this approximation hypothesis by stating that ". . . If the
velocity of the air stream which carries the eddies is very much greater than the turbulent velocity,
one may assume that the sequence of changes of u at the fixed point are simply due to the passage of
an unchanging pattern of turbulent motion over the point, i.e., one may assume that

$$u = \phi(t) = \phi(\frac{x}{\overline{U}}),\qquad(1)$$

where x is measured upstream at time $t = 0$ from the fixed point where u is measured." Here, u is the
fluctuating streamwise velocity component. This statement of his idea became known as his "frozen

---

[a]Department of Engineering Mechanics, Tsinghua University, Beijing 100084, China.
[b]Computational Fluid Dynamics Laboratory, School of Aeronautics, Universidad Politécnica de Madrid, Madrid 28040,
  Spain.
[c]Burgers Program for Fluid Dynamics and Department of Mechanical Engineering, University of Maryland, College Park,
  Maryland 20742, USA.

27, 025111-1

turbulence" hypothesis which he used to analyze grid turbulence. In essence, Taylor was stating that his approximation would be reasonably good if the time scale of changes to the turbulent field itself is large compared to the time scale of its advection downstream. For over 75 yr, experimentalists have employed this idea to circumvent the problem of probe interference from simultaneous measurements separated in the streamwise direction and for approximating spatial correlations and wavenumber spectra from temporal correlations and frequency spectra. However, they have not always observed Taylor's qualification about its limits of applicability.

There have been many further attempts to determine the limits of applicability of Taylor's hypothesis. Lin[3] imagined a probe translating through a field of homogeneous and isotropic turbulence, which is fluctuating but with no mean velocity, as the equivalent of the probe at a fixed location in advecting, uniform grid turbulence, i.e., the flow Taylor considered. In this case, Lin surmised that the hypothesis would be a good approximation if $\overline{u^2}/\overline{U}^2$ is very small. He further argued, based on a rough estimate of the magnitude of the terms in the momentum equation for the streamwise direction, that the Taylor's hypothesis approximation is reasonable for the grid turbulence case but that "... there is no general justification of extending Taylor's hypothesis to the case of shear flow." Lin made some order of magnitude estimates about how, for bounded shear flows, Taylor's hypothesis might be valid for small scales but not valid for large scales, depending on the location in the flow. Fisher and Davies[4] concluded that the convection velocity of turbulence patterns is different from the mean velocity in regions of shear flows where the turbulence intensities are large. In this case, they concluded that the distortion of the convecting eddies by the mean and fluctuating shear stresses must be taken into account. They based these observations on two-point space-time correlation measurements in a turbulent jet where they also showed that eddies of different scale advect with different velocities. The inference from this study was that a straightforward use of Taylor's hypothesis under these conditions will result in considerable error. Lumley[5] considered the mechanisms suggested by Fisher and Davies[4] for invalidating Taylor's hypothesis for high turbulence intensity shear flows, and concluded that, for small scales, only the variability of the convection velocity is important. He proposed a model to correct the high wavenumber range of one-dimensional spectra to account for this variability. Hill,[6] with applications to geophysical turbulence, and Gledzer[7] have extended Lumley's correction ideas to other statistics. Like Lin, Hekestad[8] made an order of magnitude estimate of the terms in the streamwise momentum equation, in his case for free shear flows. He assumed that the viscous forces are everywhere small compared to the pressure gradient forces, and he concluded that, for instances when the flow is negligibly accelerated by the local pressure gradient, a generalized form of Taylor's hypothesis should be valid, i.e.,

$$\frac{\partial u_i}{\partial t} + \overline{U}\frac{\partial u_i}{\partial x} + u_j\frac{\partial(\overline{U_i} + u_i)}{\partial x_j} = 0. \tag{2}$$

Here, U_i and u_i are the instantaneous and fluctuating velocity components, respectively, in the coordinate directions $x_j = x$, y, or z. Hekestad estimated that this generalized form would become more valid with increasing Reynolds number, and he found evidence for this from experiments in a turbulent jet. Tennekes[9] also took into account the additional convective acceleration term, with what has been called the "random Taylor hypothesis," in his analysis of isotropic turbulence with no mean flow. Pinsky *et al.*[10] analytically investigated the implications of the assumption underlying Taylor's hypothesis that the instantaneous Lagrangian acceleration is negligible. As had others previously, they concluded that the hypothesis becomes increasingly valid at high Taylor scale Reynolds numbers for isotropic and homogeneous turbulence. Using a multi-sensor hot-wire probe that allowed them to measure the additional fluctuating convective acceleration term, $u_j\partial(\overline{U_i} + u_i)/\partial x_j$, in Eq. (2), Loucks and Wallace[11] examined whether or not including it improved Taylor's hypothesis for turbulent boundary layer and plane mixing layer flows. Surprisingly, they found that the estimates of $\partial u/\partial x$ using the original form of Taylor's hypothesis agreed better with the values of this gradient obtained from continuity than did the estimates with Eq. (2).

Zaman and Hussain[12] compared the spatial distribution of properties of coherent structures approximated using Taylor's hypothesis applied to temporally varying hot-wire data. The properties were determined at a fixed downstream distance in a turbulent round jet, and they were compared to

those same properties determined from phase averaged data measured at variable downstream distances. They found that the hypothesis worked quite well, for positions across the jet, if the structure center velocity was used as the convection velocity. When, instead, they used the local mean velocity or the local instantaneous velocity as the convection velocity, the educed structure was considerably distorted compared to the phase averaged structure. Furthermore, they found that when the large-scale vortices in the jet were undergoing pairing, there was no convection velocity that made Taylor's hypothesis a good approximation. Browne *et al.*[13] directly estimated the fluctuating streamwise temperature gradient at the centerline of a heated plane jet using two closely spaced and very small diameter temperature sensors that they determined did not interfere with each other. They compared statistics of this directly measured temperature gradient to those estimated by applying Taylor's hypothesis to the temporal derivative of one of these signals. For the latter estimate, they tried both the mean and instantaneous velocities as the convection velocity. The choice of convection velocity had little effect on the statistics determined from the temporal derivative, and these agreed well with those determined from the spatial derivative measurement. Cendese *et al.*[14] carried out a similar study on the centerline of a rectangular duct with high turbulence intensities, where the velocity fluctuations at two locations, separated in the streamwise direction, were measured using laser-Doppler anemometry. For the closest separations, the two point spatial correlation agreed with the Taylor's hypothesis transformed temporal correlation. For larger separations, the authors observed and characterized the deformation of the turbulent fluctuations between the two locations using a transfer function analysis. Romano[15] used this experimental arrangement and type of data analysis for a turbulent channel flow at various Reynolds numbers. He extended the limits for which Taylor's hypothesis can be considered reasonably valid to bounded flows where $y^+ > 10$ and $u'/\overline{U} < 0.3$ if an optimally determined convection velocity is used in the time-space transformation. Here, u' is the root-mean-square (rms) value of the streamwise velocity fluctuations, and y^+ is the distance from the wall normalized with the viscous length scale, ν/u_τ, where ν is the kinematic viscosity and u_τ is the friction velocity. Dahm and Southerland[16] investigated Taylor's hypothesis using measurements, highly resolved in space and time, of the concentration field (fluorescence dye) in the self-similar far-field of an axisymmetric turbulent jet at its radial location of highest turbulence intensity. They could directly test the hypothesis by comparing the temporal to the streamwise spatial concentration gradients. The correlation of these gradients was 0.74 over the measurement volume. They also examined the errors in dissipation rate by comparing its value using the streamwise velocity gradient estimates from Taylor's hypothesis to their directly measured dissipation rate. L'vov *et al.*[17] did a model study of isotropic and anisotropic flow fields to assess the errors introduced by the use of Taylor's hypothesis in determining structure functions.

Recently, several experiments using current measurement technology were carried out, in part to assess the validity of using Taylor's hypothesis in various flows. For example, Ganapathisubramani[18] made time resolved stereoscopic particle image velocimetry (PIV) measurements in the cross-stream plane of a co-flowing, axisymmetric jet from which they could obtain all the velocity gradients in this plane. To estimate a volumetric rendering of this flow field, they employed Taylor's hypothesis. They did a separate set of two-dimensional (in the streamwise plane), time resolved PIV measurements to evaluated the validity of Taylor's hypothesis by comparing the streamwise and temporal gradients of the streamwise and cross-stream velocity components. Correlation coefficients of these gradients were highest at the centerline and for the cross-stream velocity component, reaching a value of about 0.89. Probability density distributions of these streamwise and temporal velocity component gradients were very similar. Very large scale motions (VLSMs), elongated in the streamwise direction for many boundary layer thickness, have been revealed in bounded turbulent flows, and they are believed to be dynamically significant. Because several studies of these VLSMs have employed Taylor's hypothesis to transform a spanwise line of velocity component temporally varying data into extended, two-dimensional, wall-parallel planes of data (see e.g., Hutchins and Marusic[19]), Dennis and Nickels[20] examined the appropriateness of doing this with time resolved PIV turbulent boundary layer data taken in the $y/\delta = 0.16$ plane, where δ is the boundary layer thickness. Because the PIV data were well resolved in time, they could compare the plane of streamwise velocity fluctuation data obtained by applying Taylor's hypothesis to the time series of a spanwise line of these data at a fixed downstream distance corresponding to the upstream end of the PIV plane, with the data from the plane

measured directly. Qualitatively, the fields looked very similar. They assessed the validity of Taylor's hypothesis quantitatively by calculating the correlation coefficient between the two planar fields. At the upstream end, their correlation coefficient was about 0.58 with the correlation falling linearly to about 0.19 at the end of the measurement plane, a distance of $x/\delta \approx 6.3$. However, by filtering out the small scales in the fields before making the correlation, they were able to boost the correlation coefficient at the upstream end of the plane to almost 0.9, a result that contradicted the speculation of Lin[3] mentioned above. Davoust and Jacquin[21] determined the optimum convection velocity for Taylor's hypothesis from time resolved, two-dimensional PIV data obtained in the cross-stream plane of an axisymmetric turbulent jet. They Fourier transformed the $\partial u/\partial x$ spatial velocity gradient, obtained from continuity of incompressible flow, and the $\partial u/\partial t$ temporal gradient. From this transformed information, they developed a method to extract the optimal convection velocity as a function of frequency. Correlation coefficients were shown as a function of radial distance from the jet centerline and of frequency. In the core of the jet and the center of the mixing layer, the correlation was high for the low frequency range, reaching values of 0.9. In the exterior of the mixing layer and for higher frequencies, the correlation coefficient dropped significantly.

All of the work cited above, that examined the assumptions underlying Taylor's hypothesis and that evaluated its validity in grid and shear flows, used estimates of the terms in the momentum equation, models to assess experimental data, and/or experimental measurements. The availability of numerical simulation data allowed such studies to be done much more directly. The first study of this sort, carried out by Piomelli *et al.*,[22] utilized a large-eddy simulation (LES) of a turbulent channel flow at low Reynolds number. They found that the correlation coefficients of the $\partial u_i/\partial t$ time derivative and the $\overline{U}\partial u_i/\partial x$ spatial derivative terms are everywhere greater than 0.9 for $y^+ > 20$, indicating a strong average phase agreement between the two from the center of the buffer layer to the channel centerline, at least for the resolved scales. Furthermore, the distributions of rms values of these terms were nearly equal for this range of y^+ values, indicating an average amplitude agreement. Kim and Hussain (KH)[23] carried out two-point space-time correlations in a low Reynolds number turbulent channel flow direct numerical simulation (DNS) to determine the convection velocities, from the wall to the channel centerline, of velocity, vorticity, and pressure fluctuations. Surprisingly, they found that the convection velocities were very nearly equal to the local mean velocity for all three types of the flow properties for $y^+ > 20$. Closer to the wall these properties convect with a nearly constant velocity which is increasingly greater than the local mean velocity as the wall is approached and is approximately equal to $10u_\tau$. They also examined the scale dependence of the convection velocities by bandpass filtering the DNS data in wavenumber space. Away from the wall, they found that there is no scale dependence, but near the wall, the convection velocities decrease significantly with increasing k_z, whereas there is only a weak dependence on k_x. Lee *et al.*[24] carried out a DNS of a compressible, isotropic turbulent flow which was homogeneous in the cross-stream directions, stationary in time, and inhomogeneous (decaying) in the mean flow direction. They also carried out a temporally evolving simulation of the same flow with the same Reynolds and Mach numbers as the spatially evolving simulation, and they compared the two flows by converting downstream distance into time for the spatially evolving case, using Taylor's hypothesis. By decomposing the flow fluctuations into their incompressible and dilatational parts, they were able to assess the validity of Taylor's hypothesis from the statistics of each part. The statistics of the incompressible part showed good agreement between the two simulations as long as the turbulence intensity was sufficiently small ($\leq 15\%$), validating the use of Taylor's hypothesis. However, the statistics of the dilatational part did not compare well between the two simulations, indicating the invalidity of Taylor's hypothesis for the compressible part of the motions. Tsinober *et al.*[25] examined the acceleration fields of a DNS of forced isotropic turbulence for a range of Taylor scale Reynolds numbers from 20 to more than 1000. For the "random Taylor hypothesis" of Tennekes,[9] described above, to be valid, they found that the ratio of the variance values of the total Lagrangian acceleration to the local and to the convective accelerations must be small, and the latter two variances should be close in magnitude to each other. At the high Reynolds number end of the range, these ratios were found to be about 0.2 or less. They also showed that the viscous force term is small compared to the pressure gradient term. The pressure gradient was found to be nearly equal to the total Lagrangian acceleration and to the potential part of the convective

acceleration. The local (temporal gradient) acceleration was nearly equal to the solenoidal part of the convective acceleration.

Tardu and Vezin[26] analyzed the terms in the streamwise momentum equation obtained from a low Reynolds number turbulent channel flow DNS to study the limitations of Taylor's hypothesis for bounded flows in a manner similar to that used in the present investigation. They concluded that Taylor's hypothesis of "frozen turbulence" is invalid in the viscous sublayer ($y^+ < 10$), is only a very crude approximation in the buffer layer ($10 < y^+ < 30$), but is a quite good approximation above these layers ($y^+ > 30$). del Alámo and Jiménez[27] have used turbulent channel flow DNS for a range of Reynolds numbers ($Re_\tau \leq 1900$) to investigate Taylor's hypothesis. Rather than determining convection velocities from space-time correlations or, correspondingly, wave-number-frequency spectra, they determined average convection velocities directly from the local time and space derivatives of the velocity field components. They also were able to examine the scale dependence of the convection velocities using only spectral information from either time or spatial direction variation and local derivatives from the other. Furthermore, they were able to derive expressions for the scale and flow location dependent convection velocities that show how they are composed of the local mean velocity and terms derived from the additional terms in the component momentum equations. They found that the convection velocities of larger scales ($\lambda_x/h \geq 2$ and $\lambda_z/h \geq 0.4$, where λ_x and λ_z are the streamwise and spanwise wavelengths, respectively, and h is the channel half-width) are nearly that of the bulk velocity over the whole flow, whereas the convection velocities of the smaller scales are closer to the local mean velocities. They also suggested that the long wavelength second peak in bimodal energy spectra obtained from experiments that employed Taylor's hypothesis may, in part, be an artifact of the errors introduced by the hypothesis. Moin[28] has provided very useful insights into many of the issues involving Taylor's hypothesis in his summary of the del Alámo and Jiménez[27] paper.

He and Zhang[29] and Zhao and He[30] have discussed Taylor's hypothesis in terms of space-time correlation for flows with a mean shear, $\overline{U}(y)$. They pointed out that the space-time correlation for separation distances r in the streamwise direction when Taylor's frozen turbulence hypothesis is invoked, i.e., $R(r,\tau) = R(r - U_c\tau, 0)$, assumes a linear space-time transformation which implies that iso-correlation correlation contours of this function are straight lines, $r - U_c t = C$, where C depends on the contour level. This had been previously observed by Wills,[31] and it is clearly incorrect because correlations decay with increasing time and space. They proposed a second-order elliptical model for the correlation at small separations, $R(r,\tau) = R(\sqrt{(r - U_c\tau^2) + V^2\tau^2}, 0)$, where the V term comes from a second-order expansion, and they call it the "sweeping" velocity. They tested this model with a low Reynolds number turbulent channel flow DNS and found that the space-time correlations collapse to a universal form throughout the flow, with the separation defined from the model, whereas this was only true in the outer part of the flow when Taylor's hypothesis was used. Furthermore, this model has been successfully applied by He *et al.*,[32] Zhou *et al.*,[33] and Hogg and Ahlers[34] in turbulent Rayleigh-Benard convection to convert temporal measurements into the spatial domain.

In this paper, we will study the limits to Taylor's hypothesis using two well resolved, in space and time, DNSs of an incompressible, steady in the mean, turbulent channel flow. The study will utilize the momentum transport equation (Navier-Stokes) for the instantaneous velocity components, U_i, i.e.,

$$\frac{\partial U_i}{\partial t} + U_j \frac{\partial U_i}{\partial x_j} = -\frac{1}{\rho}\frac{\partial P}{\partial x_i} + \nu \frac{\partial^2 U_i}{\partial x_j \partial x_j}, \tag{3}$$

where the gravitational body force term has been included in the pressure gradient term. For the flow we are considering, Eq. (3) can be written as

$$\frac{\partial u_i}{\partial t} + \overline{U}\frac{\partial u_i}{\partial x} + u_j\frac{\partial(\overline{U}_i + u_i)}{\partial x_j} = -\frac{1}{\rho}\frac{\partial(\overline{P} + p)}{\partial x_i} + \nu\frac{\partial^2(\overline{U}_i + u_i)}{\partial x_j \partial x_j}. \tag{4}$$

Equation (4) reduces to Taylor's hypothesis (the first two terms on the left-hand-side) if the mean velocity, $\overline{U}$, is a good choice of the convection velocity *and* if the additional turbulent fluctuation convective acceleration terms, $u_j\partial(\overline{U}_i + u_i)/\partial x_j$, and the pressure gradient and viscous force terms are individually instantaneously very small, or their combination is very small, when compared to

the first two terms in the equation. We will examine how and why this becomes statistically less true as the walls of bounded flows are approached, and we make observations about the degree to which this is so.

We can similarly use the vorticity transport equation for the instantaneous vorticity components, Ω_i, to study the limits of Taylor's hypothesis applied to fluctuations of vorticity. This is given by

$$\frac{\partial \Omega_i}{\partial t} + U_j \frac{\partial \Omega_i}{\partial x_j} = \Omega_j \frac{\partial U_i}{\partial x_j} + \nu \frac{\partial^2 \Omega_i}{\partial x_j \partial x_j}. \tag{5}$$

The two left-hand-side terms describe the local and convective rates of change of the vorticity of a fluid particle along its trajectory as determined by the two right-hand-side terms: stretching or compression of the particle's vorticity directly, or through reorientation by the local shear, and viscous diffusion of its vorticity. For fully developed turbulent channel flow, stationary in the mean, Eq. (5) can be written as

$$\frac{\partial \omega_i}{\partial t} + \overline{U} \frac{\partial \omega_i}{\partial x} + u_j \frac{\partial (\overline{\Omega}_i + \omega_i)}{\partial x_j} = (\overline{\Omega}_j + \omega_j) \frac{\partial (\overline{U}_i + u_i)}{\partial x_j} + \nu \frac{\partial^2 (\overline{\Omega}_i + \omega_i)}{\partial x_j \partial x_j}, \tag{6}$$

where ω_i are the vorticity component fluctuations. Analogous to the transport equation for instantaneous momentum, Eq. (6) reduces to an application of Taylor's hypothesis to the vorticity fluctuations if the mean velocity, $\overline{U}$, is a good choice of the convection velocity *and* if the additional convective rates of change terms, $u_j \partial (\overline{\Omega}_i + \omega_i)/\partial x_j$, and the stretching/compression/reorientation and viscous diffusion terms are individually and instantaneously very small, or their combination is very small, when compared to the first two terms in the equation.

Throughout this paper, lower case letters indicate fluctuations about mean values, overbars indicate those mean values, and repeated indices imply summation over the three coordinate directions. The coordinate labels x, y, and z are for the streamwise, wall normal, and spanwise directions, respectively, with corresponding velocity components U, V, and W and vorticity components Ω_x, Ω_y, and Ω_z.

II. TURBULENT CHANNEL FLOW DNS

Two turbulent channel flow datasets are used in this investigation: a new DNS performed at $Re_\tau \equiv u_\tau h/\nu = 205$ (case C200) and a higher Reynolds number simulation at $Re_\tau = 932$ (case C930) from Lozano-Durán and Jiménez,[35] where h is the channel half-width. The bulk Reynolds numbers are $Re_h = 3300$ and $18\,522$ for cases C200 and C930, respectively. Both simulations used the numerical procedure developed by Kim, Moin, and Moser.[36] Periodic boundary conditions were used in the homogeneous streamwise and spanwise directions, and no-slip boundary conditions in the wall-normal direction. The Navier-Stokes equations were numerically solved with a pseudo-spectral method, employing Fourier series in both the streamwise and spanwise directions, and Chebyshev polynomial expansions in the wall-normal direction. For both simulations, the grid is uniform in the streamwise and spanwise directions, and the points are closely concentrated in the wall normal direction near both walls by using $y_j = \cos[(j-1)/(N_y - 1)\pi]$, where $j = 1 - N_y$ and N_y is the number of grid points in that direction. The aliasing errors were removed by using the 3/2-rule. Time was advanced with a second-order, stiffly stable scheme following that of Karniadakis *et al.*,[37] for case C200, and with a third-order semi-implicit Runge-Kutta from Spalart *et al.*[38] for case C930. Table I summarizes the main parameters of the simulated flows.

The spatial resolution in both cases (Table I) is similar to the resolution used in the previous investigations, and it has proved to be good enough to capture the dynamics of the smallest scales of the flow (see, for instance, Jiménez and Moin[39]). Case C200 was run with a fixed time step equal to 1/200 viscous time units and was used to calculate time derivatives, assuring temporal accuracy. The maximum Courant-Friedricks-Lewey (CFL) number reached was 0.2. Case 930 was run with a fixed CFL number of 0.5, and a smaller CFL of 0.05 was used to generate an extra flow field to compute the time derivatives. In all cases, the CFL numbers remained within the range where there were no numerical spurious behaviors (see Jiménez[40] and Jiménez and Moin[39]).

TABLE I. Summary of the main parameters of the simulations. Re_h and Re_τ are the bulk and friction Reynolds numbers, respectively. Δx and Δz denote the streamwise and spanwise resolutions, and Δy_{min} and Δy_{max} the maximum and minimum wall normal resolutions, respectively. N_x, N_y, and N_z are the number of collocation points in the streamwise, wall normal, and spanwise directions, respectively. Δt^+ is the averaged time step to advance the Navier-Stokes equations in the DNSs.

Case	Re_h	Re_τ	Δx^+	Δy_{min}^+	Δy_{max}^+	Δz^+	N_x	N_y	N_z	Δt^+
C200	3,300	205	13	0.06	5.0	7	64	129	32	0.012
C930	18,522	932	11.5	0.031	7.6	5.7	768	385	768	0.026

The computational domains of the present DNSs were $1.3\pi h \times 2h \times 0.35\pi h$ for case C200 and $2\pi h \times 2h \times \pi h$ for case C930 in the streamwise, wall normal, and spanwise directions. The first domain is twice as long as that of Vukoslavčević *et al.*,[41] who used a turbulent channel flow DNS to study simulated multi-sensor hot-wire probe resolution. The domain for case C930 is even larger, and both simulation domains were shown to produce correct one-point statistics,[35] as demonstrated below.

Statistics of these two simulations were compared to those of Kim *et al.*[36] and Vukoslavčević *et al.*[41] at similar low Reynolds numbers to our low Reynolds number simulation of $Re_\tau = 205$, with an excellent agreement. To show that this is true for both large scale and small scale properties, the distributions across the half-width of the channel for the production rate and the full dissipation rate are shown in Fig. 1. These properties have only slightly larger values throughout the flow for the $Re_\tau = 932$ simulation than those for the low Reynolds number simulations. Here and elsewhere, + indicates normalization with viscous scales.

The primary reason that we initially conducted this study using a low Reynolds number channel flow DNS is that our sole purpose was to study in detail the physical processes, as given by the transport equations, that cause Taylor's hypothesis to become inaccurate as the wall is approached. This obviously can be done effectively at low Reynolds number with less computational cost than at higher Reynolds number. We anticipated that the only effect of increasing the Reynolds number is that the region where Taylor's hypothesis significantly breaks down will be a smaller portion of the total flow. Indeed, at infinite Reynolds number, this region will be vanishingly thin. Thus, we reasoned, the low Reynolds number case is the worse case that can be studied. However, to be sure that the results at low Reynolds number still hold at higher Reynolds numbers, we carried out the same analysis on the higher Reynolds number DNS at $Re_\tau = 932$. As anticipated, there were no significant changes required to the conclusions drawn from this latter analysis.

A secondary reason for carrying out the study at $Re_\tau = 205$ was that this allowed us to directly compare the convection velocities described in Sec. III with those calculated by Kim and Hussain[23] in a quite different way, but at a very similar low Reynolds number. Also, it allowed us to compare the correlation coefficients for the velocity derivatives, described in Sec. IV, with those calculated
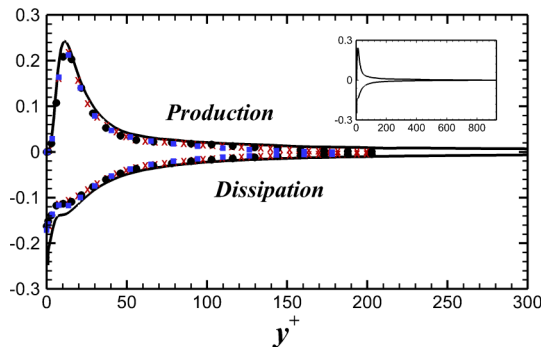

FIG. 1. Production and dissipation rates for turbulent channel flow, normalized with u_τ^4/ν: solid lines and filled circles (black online), present data for $Re_\tau = 932$ and 205, respectively; crosses (red online), Vukoslavčević *et al.*:[41] filled squares (blue online), Kim *et al.*[36]

from a LES by Piomelli *et al.*[22] at about the same Reynolds number. The comparisons have been kept, and the higher Reynolds number results have been added to them. However, except for the figures showing these comparisons, all the remaining figures show only the higher Reynolds number results. These higher Reynolds number figures are very similar to the same types of figures, not shown, where the lower Reynolds number results were plotted.

III. CONVECTION VELOCITIES

Although the local mean velocity has often been used as the convection velocity, U_c, for Taylor's hypothesis, it was shown by Zaman and Hussain,[12] Kim and Hussain,[23] and others that this is not the best choice for all locations in turbulent shear flows. As noted above, for channel flows, Kim and Hussain[23] found that, near walls for y^+ less than about 20, the convection velocities of turbulent fields are nearly constant and equal to each other with values of about $10u_\tau$, while the local mean velocity drops to zero at the wall. Above y^+ of about 20, the convection and local mean velocities are approximately equal. They determined the convection velocities for the velocity and vorticity components and pressure fields from space-time correlations by calculating the quotient, given by the separation distance for maximum correlation, divided by a fixed time delay.

A. Velocity fluctuations

In our investigation, we determine the convection velocities for the velocity component fluctuations quite differently by using local values of $-\partial u_i/\partial t$ and $\partial u_i/\partial x$, as was previously done by del Alámo and Jiménez.[27] Fig. 2 is a scatter plot of these two derivatives for the u component at $y^+ = 5$, where, it will later be shown, a measure of the error in Taylor's hypothesis, with a convection velocity that includes all scales, is near its peak. The solid line plotted is the linear least sum of the mean square differences fit of the data. The slope of this line is the inverse of the average convection velocity, $1/U_{cu}$. It is rather straightforward to show that the values of U_{cu_i} for each of the component directions, obtained graphically in this manner, are the same as those that minimize the mean square differences between $U_{cu_i}(\partial u_i/\partial x)$ and $-\partial u_i/\partial t$. This is done by differentiating these differences, for each component direction, with respect to U_{cu_i}, setting the derivatives to zero, and then solving for the U_{cu_i} values which are given by

$$U_{cu_i} = \frac{\overline{(-\partial u_i/\partial t)\,(\partial u_i/\partial x)}}{\overline{(\partial u_i/\partial x)^2}}. \tag{7}$$
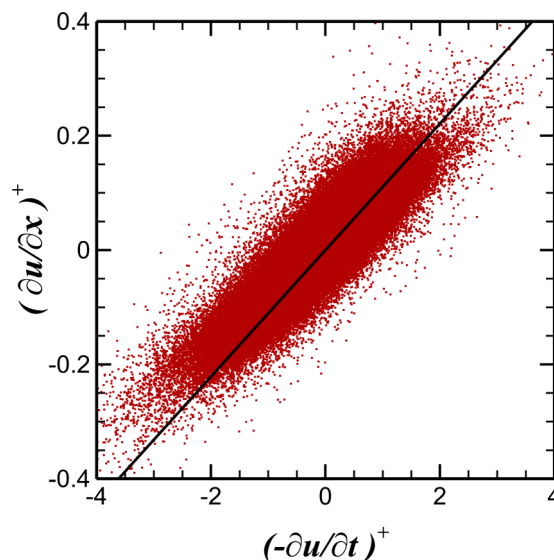

FIG. 2. Scatter plot of $(\partial u/\partial x)^+$ vs. $(-\partial u/\partial t)^+$ for $y^+ = 5$ at $Re_\tau = 932$. Solid line, linear least-square fit with slope $1/U_{cu}$.

This expression for the convection velocities also was previously derived by del Alámo and Jiménez.[27] The numerator of this formula for U_{cu_i} is simply the covariance of the two derivatives (their correlation), and the denominator is the variance of the streamwise spatial derivative.

It is also easy to show that, if the correlation coefficients of the two derivatives are unity, then the mean square differences between $U_{cu_i}(\partial u_i/\partial x)$ and $-\partial u_i/\partial t$, with optimized U_{cu_i}, are zero, and the optimized values of U_{cu_i} are, alternatively, given by the ratios of the rms values of $-\partial u_i/\partial t$ to those of $\partial u_i/\partial x$. If the correlation coefficients are less than unity, the convection velocities are these correlation coefficients times the values of these rms ratios, and there is a residual nonzero value of their minimized mean square differences. Values of the convection velocities, U_{cu_i}, determined with Eq. (7), or in this equivalent manner with the correlation coefficients, may be viewed simply as scaling factors that rescale the amplitudes of $\partial u_i/\partial x$ to match, as closely as possible, in a mean square difference sense, with those of $-\partial u_i/\partial t$.

In Fig. 3, the values of the convection velocities for the three velocity component fields, calculated with Eq. (7) for both simulations, are compared to the values found by Kim and Hussain[23] with space-time correlations. The agreement is remarkably good between the results from our simulations and that of Kim and Hussain[23] in spite of the differences in the methods used to determine the convection velocities. As noted in the Introduction, for $y^+ > 20$, the convection velocities for each of the velocity components are close to each other and to the local mean velocity. Below this location, the convection velocities are increasingly larger than the local mean velocity as the wall is approached. For $y^+ < 5$, in the viscous sublayer, the convection velocities of all three velocity fluctuations are very nearly constant, with a value of about $10u_\tau$ for the lower Reynolds number case and between about $9u_\tau$ and $10u_\tau$ for the higher Reynolds number case.

Fig. 4 shows the joint probability density functions (JPDFs) of $U_{cu}\partial u/\partial x$ and $-\partial u/\partial t$ at $y^+ = 5$, 12, 50 and the channel centerline, $y^+ = 932$, for the higher Reynolds number case, with U_{cu} determined as described above. The slopes of the solid lines on the plots are unity, corresponding to the loci of pairs of values and their probabilities where $U_{cu}\partial u/\partial x$ and $-\partial u/\partial t$ are identically equal. The dotted points in the plots are along the ridge, defined by the peak probability densities of the JPDFs, for varying values of $-\partial u/\partial t$. These peak probability ridges are nearly coincident with the solid lines where there are sufficient data to define smoothly varying surfaces of the JPDFs. Also shown in the plots are dashed lines corresponding to the equality of $(1 \pm 0.2)U_{cu}\partial u/\partial x$ and $-\partial u/\partial t$. At the channel centerline, the region between these dashed lines includes much, but not all, of the instantaneous data, especially for the larger magnitude pairs of values. However, near the wall at $y^+ = 5$, 12, and even at 50, much of the instantaneous data falls outside of this region. The JPDFs of the v and w velocity component derivatives, and for the lower Reynolds number case, are very similar for the same y^+ locations.
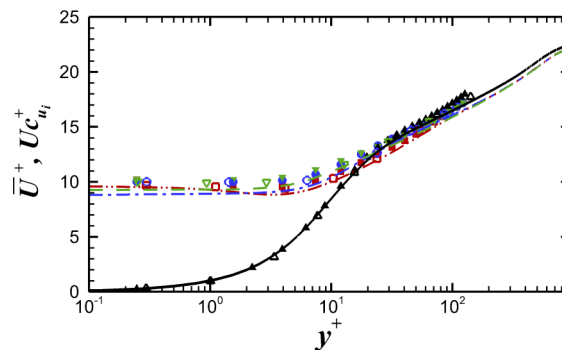

FIG. 3. Comparison of distributions of the convection velocities of the velocity component fluctuations between the present investigation at higher and lower Reynolds numbers and that of KH.[23] U_{cu}^+: dashed-dotted-dotted-dashed ($Re_\tau = 932$) and filled squares ($Re_\tau = 205$), present; open squares, KH (all red online). U_{cv}^+: dashed-dotted-dashed and filled circles, present; open circles, KH (all blue online). U_{cw}^+: dashes and filled inverted triangles, present; open inverted triangles, KH (all green online), $\overline{U}^+$: solid line and filled triangles, present; open triangles, KH (all black online).
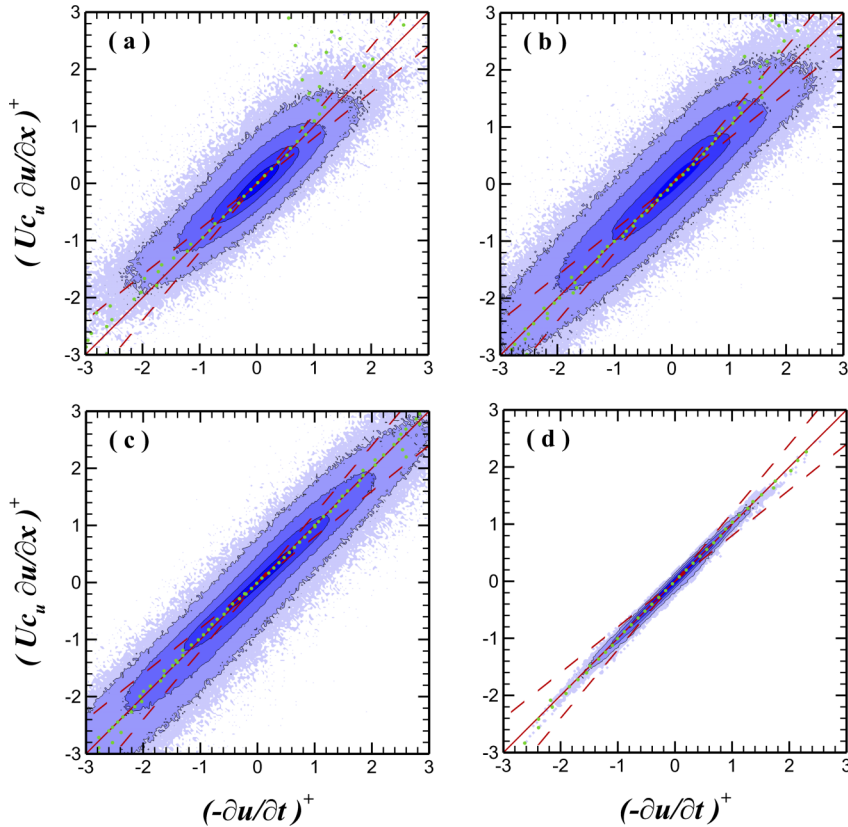
FIG. 4. JPDFs of $(U_{c_u}\partial u/\partial x)^+$ and $(-\partial u/\partial t)^+$ at (a) $y^+ = 5$, (b) $y^+ = 12$, (c) $y^+ = 50$, and (d) $y^+ = 932$, the channel centerline. Solid lines (red online), for equality of the two variables with convection velocity of U_{c_u}; dashed lines (red online), for equality of the two variables with convection velocities of $U_{c_u}(1 \pm 0.2)$. Dots (green online), locations of maximum probability density for varying values of $(-\partial u/\partial t)^+$.

B. Vorticity fluctuations

The convection velocities for the three vorticity component fluctuation fields can be calculated similarly to those for the velocity fluctuations by substituting ω_i for u_i in Eq. (7). In Fig. 5, the values of these convection velocities for the vorticity component fluctuation fields are also compared to the values found by Kim and Hussain[23] from space-time correlations. As for the comparison of the
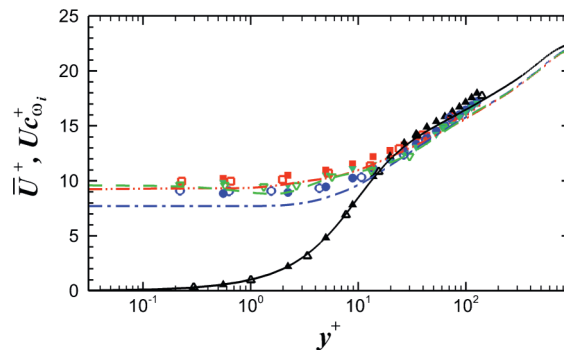

FIG. 5. Comparison of distributions of the convection velocities of the vorticity components between the present investigation at higher and lower Reynolds numbers and that of KH.[23] $U_{c\omega_x}^+$: dashed-dotted-dotted-dashed ($Re_\tau = 932$) and filled squares ($Re_\tau = 205$), present; open squares, KH (all red online). $U_{c\omega_y}^+$: dashed-dotted-dashed and filled circles, present; open circles, KH (all blue online). $U_{c\omega_z}^+$: dashes and filled inverted triangles, present; open inverted triangles, KH (all green online). $\overline{U}^+$: solid line and filled triangles, present; open triangles, KH (all black online).

velocity field fluctuations in Fig. 3, the agreement for the vorticity field fluctuations is remarkably good throughout the flow. Also, as for the velocity component fluctuations, these convection velocities are nearly equal to the local mean velocity for $y^+ > 20$, and they become nearly constant, with values of between about $9u_\tau$ and $10u_\tau$ for the lower Reynolds number case and between about $8u_\tau$ and $10u_\tau$ for the higher Reynolds number case, as the wall is approached, i.e., close to the values for the velocity components in this near wall region.

Fig. 6 shows the JPDFs of $U_{c\omega_x}\partial\omega_x/\partial x$ and $-\partial\omega_x/\partial t$, normalized by the square of the viscous time scale, at $y^+ = 5$, 12, 50, and 932, the channel centerline for the higher Reynolds number case. These JPDFs for the streamwise vorticity field derivatives have very similar properties as those for the streamwise velocity field derivatives shown in Fig. 4. The JPDFs of the ω_y and ω_z vorticity component derivatives, and for the lower Reynolds number case, are similar to those of the ω_x streamwise component for the same y^+ locations, as also is the case, noted above, for the velocity component derivatives.

IV. CORRELATION COEFFICIENTS

A. Velocity fluctuations

The correlation coefficients of $\partial u_i/\partial t$ and $U_{cu_i}\partial u_i/\partial x$, given by

$$R_{\partial u_i} = \frac{\overline{(-\partial u_i/\partial t)(\partial u_i/\partial x)}}{[\overline{(-\partial u_i/\partial t)^2}]^{\frac{1}{2}}[\overline{(\partial u_i/\partial x)^2}]^{\frac{1}{2}}}, \tag{8}$$
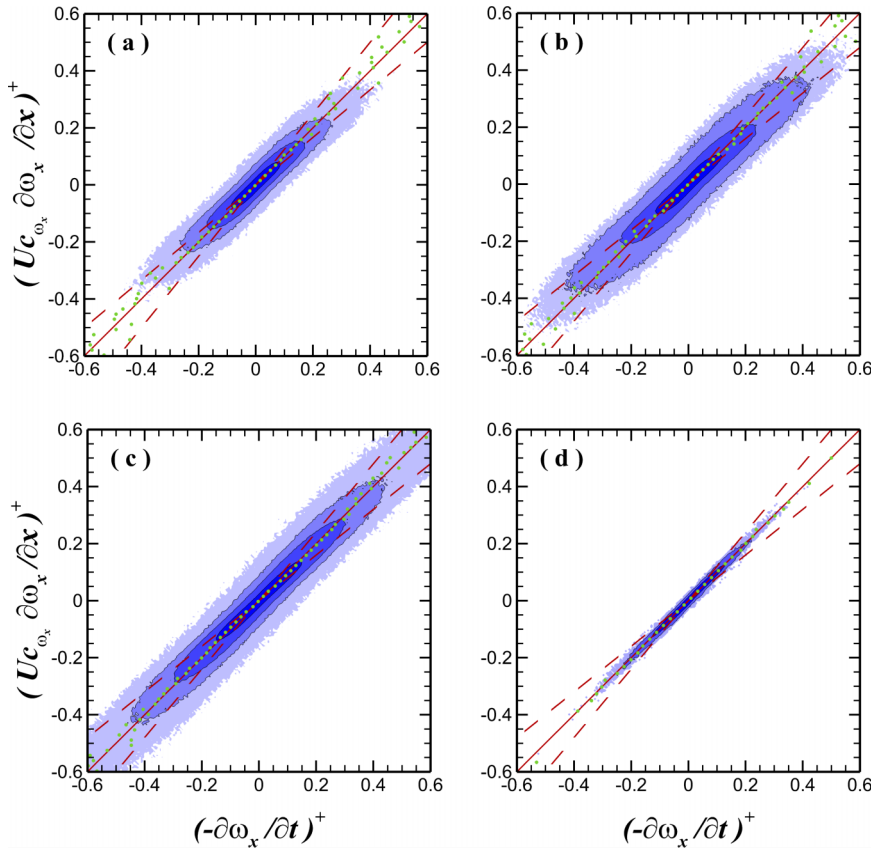

FIG. 6. JPDFs of $(U_{c\omega_x}\partial\omega_x/\partial x)^+$ and $(-\partial\omega_x/\partial t)^+$ at (a) $y^+ = 5$, (b) $y^+ = 12$, (c) $y^+ = 50$, and (d) the channel centerline, $y^+ = 932$. Solid lines (red online), for equality of the two variables with convection velocity of $U_{c\omega_x}$; dashed lines (red online), for equality of the two variables with convection velocities of $U_{c\omega_x}(1 \pm 0.2)$. Dots (green online), locations of maximum probability density for varying values of $(-\partial\omega_x/\partial t)^+$.
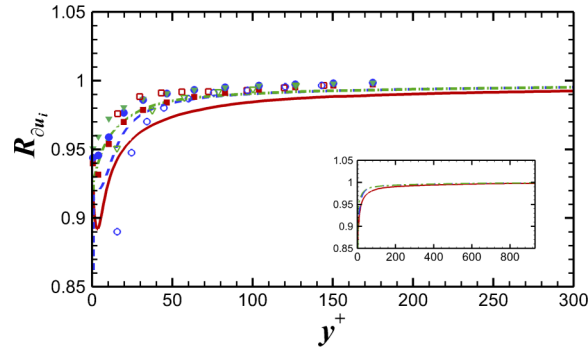
FIG. 7. Comparison of the distributions of correlation coefficients, $R_{\partial u_i}$, of $\partial u_i/\partial t$ and $U_{c u_i}\partial u_i/\partial x$ from this investigation for the higher and lower Reynolds number cases with those from Piomelli *et al.*[22] (PBW). $R_{\partial u}$: solid line ($Re_\tau = 932$) and filled squares ($Re_\tau = 205$), present; open squares, PBW (all red online). $R_{\partial v}$: dashes, and filled circles, present; open circles, PBW (all blue online). $R_{\partial w}$: dashed-dotted and filled inverted triangles, present; open inverted triangles, PBW (all green online).

are the measures of the average phase alignment of time histories of these terms because the instantaneous amplitudes of the two correlated signals are normalized by their respective rms values, which removes, on average, the effect of the differences in the signal amplitudes on the correlations. As described in the Introduction, Piomelli *et al.*[22] calculated the correlation coefficients for the three velocity components using data from a turbulent channel flow LES at a Reynolds number $Re_\tau = 157$. In Fig. 7, their values are compared to those calculated from our higher and lower Reynolds number DNSs. It is clear from our data that the two signals are highly correlated over the entire channel half-width, with correlation coefficient values greater than about 0.97 for all three components when $y^+ > 50$. The correlation coefficient values from our DNS for the u fluctuations are the smallest, but the values are still everywhere greater than about 0.89, even very near the wall. These results agree rather well with those of Piomelli *et al.*[22] except that their correlation coefficient values differ in the buffer layer where the lack of resolution of the small scales by the LES and the use of subgrid scale modeling is evident.

B. Vorticity fluctuations

The correlation coefficients of the temporal and streamwise spatial derivative terms in Taylor's hypothesis for the vorticity fluctuations, ω_i, are shown in Fig. 8 for which there is no comparison data. For $y^+ > 30$, the correlation coefficients for all three vorticity components are greater than 0.96. Nearer to the wall than this, in the buffer and sublayers, these coefficients decrease, but they never fall
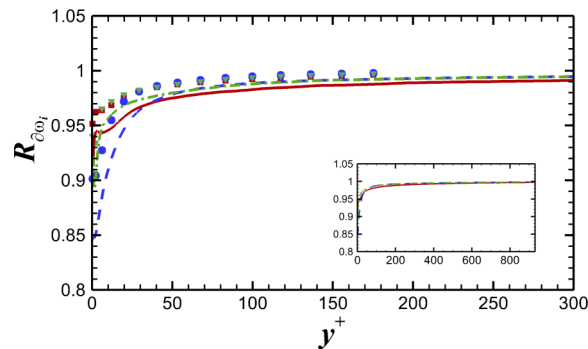

FIG. 8. Distributions of correlation coefficients at higher and lower Reynolds numbers, $R_{\partial \omega_i}$, of $-\partial \omega_i/\partial t$ and $U_{c \omega_i}\partial \omega_i/\partial x$. $R_{\partial \omega_x}$, solid line ($Re_\tau = 932$) and filled squares ($Re_\tau = 205$) (red online); $R_{\partial \omega_y}$, dashes and filled circles (blue online); $R_{\partial \omega_z}$, dashed-dotted and filled inverted triangles (green online).

below about 0.9 for the wall normal and spanwise components, and are never lower than about 0.85 for the streamwise component. Thus, as for the velocity fluctuations, this indicates a good average phase agreement between $-\partial \omega_i/\partial t$ and $U_{c\omega_i}\partial \omega_i/\partial x$, even very near the wall.

V. TRANSPORT EQUATIONS ANALYSES

A. Momentum

The momentum transport equation (4) can be further rearranged as

$$\overline{U}\frac{\partial u_i}{\partial x} = -\frac{\partial u_i}{\partial t} - \frac{1}{\rho}\frac{\partial(\overline{P}+p)}{\partial x_i} + \nu\frac{\partial^2(\overline{U_i}+u_i)}{\partial x_j \partial x_j} - u_j\frac{\partial(\overline{U_i}+u_i)}{\partial x_j}, \tag{9}$$

where now, as stated above, if the pressure and viscous force terms and the additional turbulent fluctuation convective acceleration terms on the right-hand-side are instantaneously very small, or their sum is very small, compared to the local acceleration term (the first term on the right-hand-side of the equation), then Taylor's hypothesis is quite well satisfied in the region of the flow where the convection velocity is nearly equal to the mean velocity, i.e., $y^+ > 20$.

We also can determine, from the data in Fig. 3, empirical functions of y^+ that are the differences between the convection velocities for the velocity components and the mean velocity,

$$f_{u_i}(y^+) = U_{cu_i} - \overline{U}, \tag{10}$$

and substitute for $\overline{U}$ in Eq. (9) to obtain the following:

$$\frac{\partial u_i}{\partial x}\bigg|_I = \frac{1}{U_{cu_i}}[-\frac{\partial u_i}{\partial t}\bigg|_{II} - \frac{1}{\rho}\frac{\partial(\overline{P}+p)}{\partial x_i}\bigg|_{III} + \nu\frac{\partial^2(\overline{U_i}+u_i)}{\partial x_j \partial x_j}\bigg|_{IV} - u_j\frac{\partial(\overline{U_i}+u_i)}{\partial x_j}\bigg|_V + f_{u_i}\frac{\partial u_i}{\partial x}\bigg|_{VI}]. \tag{11}$$

All the terms in Eq. (11) have zero mean values except for terms III, IV, and V, so when Eq. (11) is averaged it becomes

$$\frac{1}{U_{cu_i}}(-\frac{1}{\rho}\frac{\partial\overline{P}}{\partial x_i} + \nu\frac{\partial^2\overline{U_i}}{\partial x_j \partial x_j} - \overline{u_j\frac{\partial u_i}{\partial x_j}}) = 0. \tag{12}$$

The first two terms in Eq. (12), applied to the streamwise direction, are the forces due to the mean streamwise pressure gradient, $-\partial\overline{P}/\partial x$, and the mean viscous shear stress, $\nu\partial^2\overline{U}/\partial y^2$, respectively. The mean value of the third term for the streamwise component equation is $-\overline{v\partial u/\partial y}$, i.e., the mean additional convective acceleration due to the turbulent fluctuations in the wall normal direction. An equivalent form and alternative interpretation of this term are that it is the wall normal gradient of the Reynolds shear stress, $-\partial\overline{uv}/\partial y$. When Eq. (11) is applied to the wall normal direction, only terms III and V have non-zero mean values, and they are the wall normal gradients of the pressure and mean square wall normal velocity fluctuations which are equal to each other, i.e., $-\partial\overline{P}/\partial y = \partial\overline{v^2}/\partial y$. All the terms in Eq. (11) when applied to the spanwise direction have zero mean values. Therefore, the net effect of the mean values of terms III-VI in Eq. (11) on Taylor's hypothesis for all three directions is zero.

This is demonstrated in Fig. 9 where the mean values of these terms in Eq. (11), applied to each of the coordinate directions, are shown. Here, and in the rest of the paper, only the results from the higher Reynolds number case are plotted. All the results from the lower Reynolds number case (not shown) are quite similar. In Fig. 9(a), the negative mean of the viscous stress term, IV, increases sharply in the buffer layer and peaks very near the wall. However, it is offset in this region by the sharply rising mean of the additional convective acceleration term (the gradient of the Reynolds shear stress), term V, so that the mean of the sum of terms III-VI is zero all across the channel. This zero sum is also clear in Fig. 9(b), which shows that the wall normal gradients of pressure and mean square wall normal velocity fluctuations are equal and opposite, and in Fig. 9(c), where all the means of the terms in Eq. (11), applied to the spanwise velocity, are zero throughout the channel.
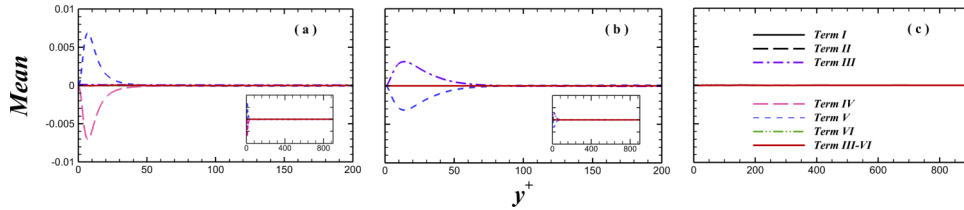
FIG. 9. Distributions of the mean values, normalized with u_τ, of individual terms I-VI and the mean values of the sum of terms III-VI from Eq. (11) for the (a) streamwise, (b) wall normal, and (c) spanwise velocity components, all with the same vertical scale. Lines: solid (black online), I; long dashes (black online), II; long-short dashes (purple online), III; long dashes (red online), IV; short dashes (blue online), V; dashed-dotted-dotted-dashed (green online), VI; also solid (scarlet online), sum of III-VI. All the other terms that have zero mean values for all y^+ values are hidden in these plots by these sum of terms III-VI curves in the three plots.

When Eq. (12) is subtracted from Eq. (11), the remainder is

$$\frac{\partial u_i}{\partial x}_I = \frac{1}{U_{c u_i}}\{-\frac{\partial u_i}{\partial t}_{II} - \frac{1}{\rho}\frac{\partial p}{\partial x_i}_{III} + \nu\frac{\partial^2 u_i}{\partial x_j \partial x_j}_{IV} - [u_j\frac{\partial(\overline{U}_i + u_i)}{\partial x_j} - \overline{u_j\frac{\partial u_i}{\partial x_j}}]_V + f_{u_i}\frac{\partial u_i}{\partial x}_{VI}\}. \tag{13}$$

The streamwise spatial and temporal derivative terms on either side of the equal sign (I and II) in Eq. (13) are clearly those in Taylor's hypothesis, expressed using the inverse of the optimized values of the convection velocities, $1/U_{c u_i}$, obtained with Eq. (7) and that include all scales and depend on y^+. Thus, to reiterate, the hypothesis will be instantaneously quite well satisfied for the velocity field fluctuations if each of the additional terms on the right-hand-side (III-VI) are instantaneously and individually quite small compared to term II, or if they combine so that their sum is instantaneously quite small compared to term II.

1. Average amplitudes of terms in Eq. (13)

Because these instantaneous terms in Eq. (13) can have both positive and negative values which can cancel each other, their average amplitudes can be determined best with their rms values. The distributions of these rms values of the two Taylor's hypothesis terms, I and II, the individual terms III-VI and the sum of terms III-VI from Eq. (13) for each of the three velocity components are plotted in Figs. 10(a)–10(c). Note that the instantaneous values of the sum of terms III-VI include the instantaneous signs of the terms in the sum, so cancelation between terms can occur. Thus, the rms of this instantaneous sum of terms III-VI is a measure of the average amplitude of the combination of terms that diminish the validity of Taylor's hypothesis. The inset in the figure magnifies the values of the distributions for $y^+ < 10$.

The relative magnitudes of the rms values of the terms in Eq. (13), applied for the three coordinate directions, are shown in Figs. 10(d)–10(f) where the distributions of the ratios of the rms values of the convective acceleration term I, the individual terms III-VI and the sum of terms III-VI to the rms values of the local acceleration term II are plotted. At $y^+ \geq 50$, the average amplitude of the ratio of the sum of terms III-VI to term II is only a little greater than 20% of the ratio of term I to term II for the streamwise component equation and less than 20% for the wall normal and spanwise component equations. These percentages diminishes even more further toward the channel centerline. On the other hand, in the viscous sublayer, the average amplitude of the ratio of the sum of terms III-VI to term II is more than 50% of the ratio of term I to term II for the streamwise equation, indicating that Taylor's hypothesis is a poor approximation in this region. Here, as the wall is approached, terms III and IV, representing pressure gradient and viscous forces, become considerably larger than terms I and II, as shown in the inset, and term VI, representing the effect of the differences between the convection velocities and the mean velocity, becomes as large as terms I and II. The comportment in the viscous sublayer of the terms for the wall normal and spanwise equations is similar to that for the streamwise equation.
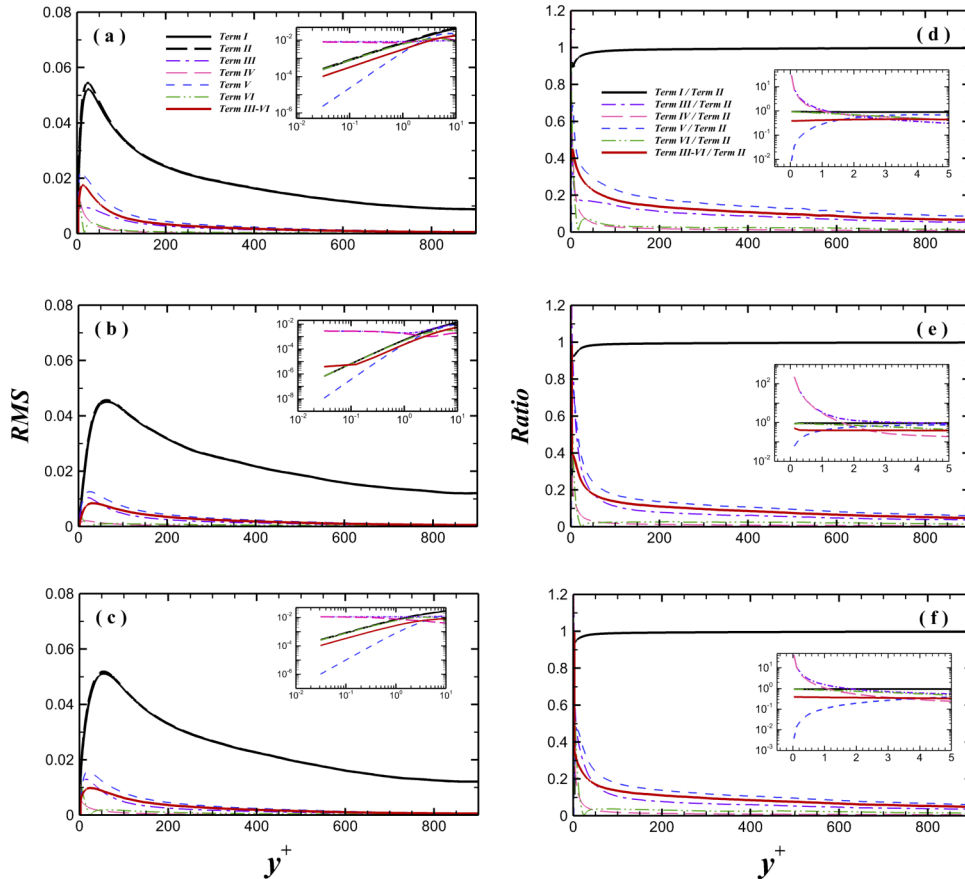
FIG. 10. Distributions of rms values, normalized with u_τ, of individual terms I-VI and the sum of terms III-VI from Eq. (13) applied for the (a) streamwise, (b) wall normal, and (c) spanwise directions. Lines: upper solid (black online), I; upper long dashes (black online), II; long-short dashes (purple online), III; lower long dashes (red online), IV; short dashes (blue online), V; dashed-dotted-dotted-dashed (green online), VI; lower solid (scarlet online), sum of III-VI. Distributions of the ratios of the rms values of terms I, III-VI and the sum of terms III-VI to the rms values of term II from Eq. (13) applied for the (d) streamwise, (e) wall normal and (f) spanwise directions. Lines: upper solid (black online), I/II; long-short dashes (purple online), III/II; long dashes (red online), IV/II; short dashes (blue online), V/II; dashed-dotted-dotted-dashed (green online), VI/II; lower solid (scarlet online), sum of (III-VI)/II.

2. Probability density functions (PDFs) of the ratio of terms in Eq. (13)

Fig. 9 gives information about the average values of the terms in momentum equation (11) applied to the three coordinate directions, and Figs. 10(a)–10(f) gives information about the relative average amplitudes of these terms, as expressed in Eq. (13) and indicated by the rms values of their fluctuations. Additionally, however, it is of interest to know how the probabilities of the instantaneous values of the amplitudes of the fluctuating terms in Eq. (13) are distributed.

In Fig. 11, the PDFs, for $y^+ = 5$, 12, 50, and 932 (the channel centerline), are shown of the instantaneous ratios, defined by term I, the individual terms III-VI and the sum of terms III-VI, all divided by term II, where these terms are defined in Eq. (13). The patterns of the PDFs of these ratios of the terms for all three component equations are similar to each other. At the centerline, all the PDFs are narrow compared to those near the wall, and the PDFs of the ratio of the Taylor's hypothesis terms, I/II, have most probable values at or very near ratios of unity at the centerline, whereas the most probable values of the PDFs of the ratios of the other terms, compared to term II, are near zero. These observations make it clear that Taylor's hypothesis is a quite good, although not perfect (as indicated by the spread of the PDFs and the other evidence already noted above), approximation at and near the channel centerline. Much closer to the wall at $y^+ = 5$ and 12, the PDFs of all the terms
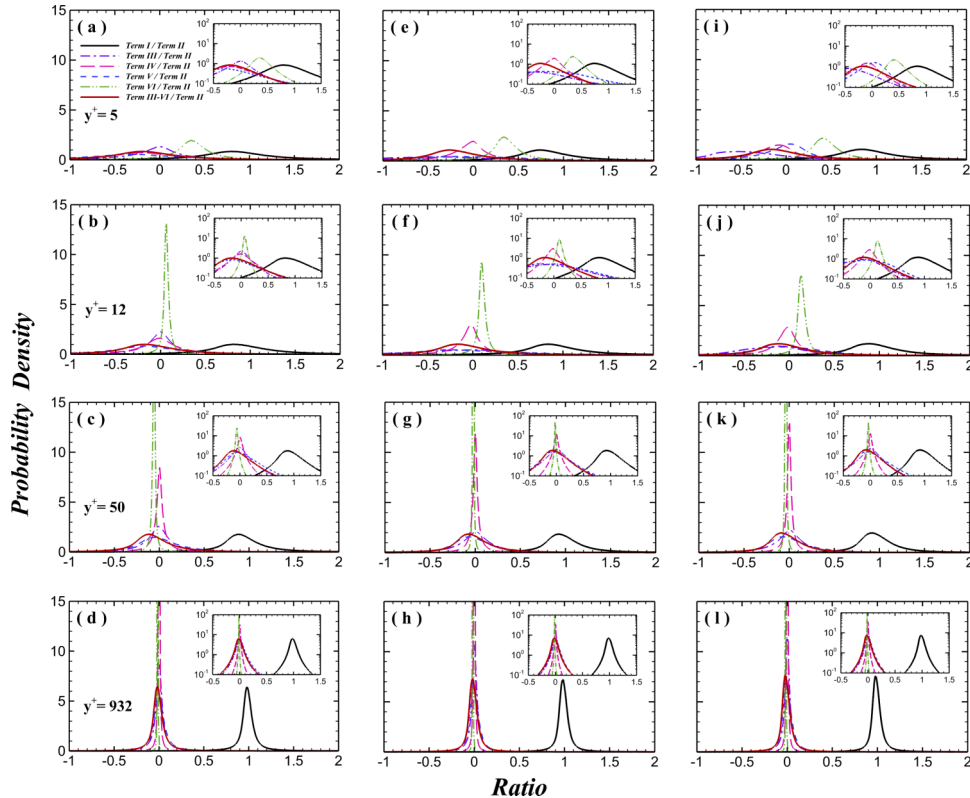
FIG. 11. PDFs of the ratios of terms I, III-VI and the sum of III-VI to term II of Eq. (13) applied to the three velocity components. From left to right: (a)–(d) streamwise, (e)–(h) wall normal, and (i)–(l) spanwise velocity components and from top to bottom, $y^+ = 5$, $y^+ = 12$, $y^+ = 50$, and the channel centerline, $y^+ = 932$. Lines: right solid (black online), I/II; long-short dashes (purple online), III/II; long dashes (red online), IV/II; short dashes (blue online), V/II; dashed-dotted-dotted-dashed (green online), VI/II; left solid (scarlet online), sum of (III-VI)/II.

are much broader. It is clear that the probability is high that the ratio of the Taylor's hypothesis terms, I/II, can be significantly different from unity in this high mean shear region because the ratio of the sum of the other terms to term II, i.e., (III-VI)/II, can be significantly different from zero. In fact, for all three component equations, the most probable values of the ratio of terms I/II are not at unity and the most probable values of the ratio of the sum of III-VI/II are quite a bit different from zero at these near wall positions. At $y^+ = 50$, the PDFs just begin to show characteristics that are more like those at the centerline than those nearer the wall. This is consistent with the conclusions drawn from the rms information in Fig. 10. The PDFs at these four locations also show how the values of the individual terms III-VI are distributed with respect to the distribution of the sum of their instantaneous values. Noteworthy is the strong effect that term VI has on diminishing the validity of Taylor's hypothesis at $y^+ = 5$. The most probable ratio of term VI to term II is only a little less than 0.5 there for all three component equations. Recall that term VI accounts for the fact that the local mean velocity is much less than the optimal convection velocity very near the wall.

3. Instantaneous x-direction distributions of values of the terms in Eq. (13)

To visualize how these terms affect the instantaneous validity of Taylor's hypothesis, lines of instantaneous data, for the terms in the streamwise component of Eq. (13), are plotted in Fig. 12 for $y^+ = 5$, 12, 50, and 932 in the x-direction along the centers of these homogeneous planes. The left-hand-side of the figure shows the degree of correspondence between terms I and II of Taylor's hypothesis, $\partial u / \partial x$ and $1/U_{cu} \partial u / \partial t$, from the channel centerline to very near the wall. Clearly, in the center of the channel, the agreement is visually almost perfect, and even at $y^+ = 50$, it is rather
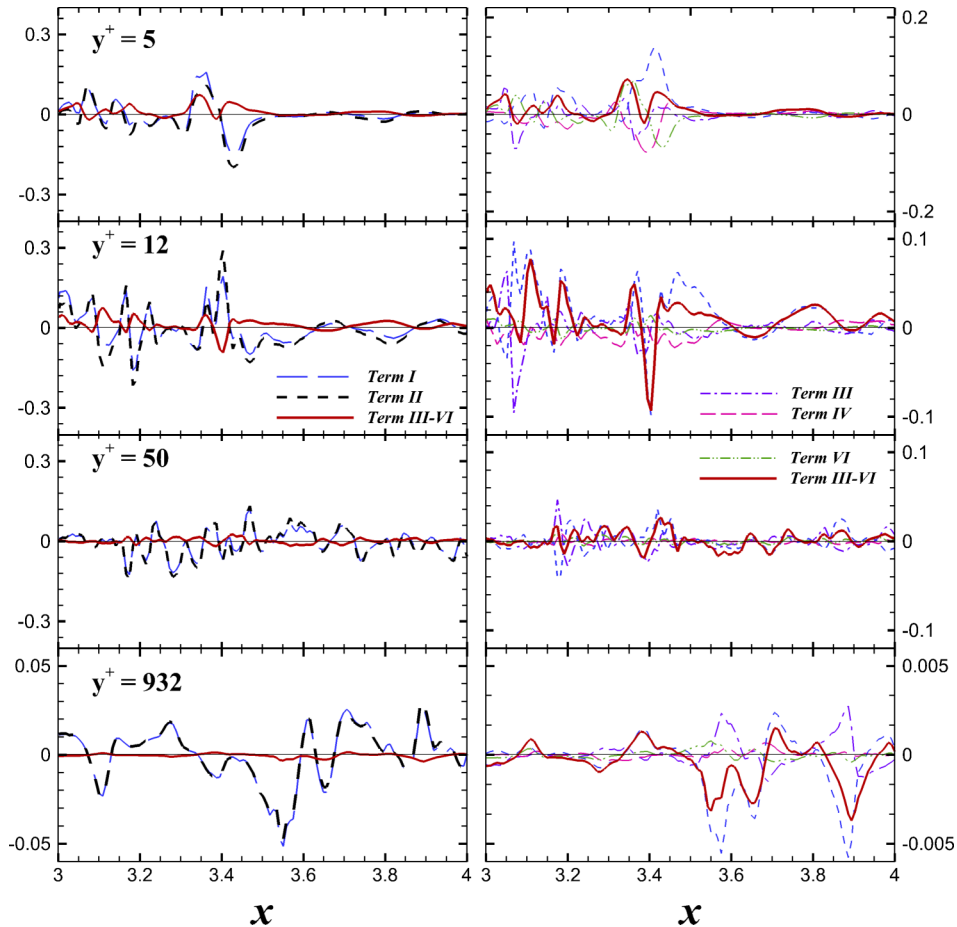
FIG. 12. Streamwise lines of data, at $y^+ = 5$, 12, 50, and 932 (the channel centerline), for terms in Eq. (13) for the streamwise velocity component. Lines left-hand-side: long dashes (blue online), I; short dashes (black online), II; solid (scarlet online), sum of III-VI. Lines right-hand-side: solid (scarlet online), sum of III-VI; long-short dashes (purple online), III; dashes (red online), IV; short dashes (blue online), V; dashed-dotted-dotted-dashed (green online), VI. Note the change in vertical scale of plots on the right-hand-side of this figure and for the lower plot on the left-hand-side.

good. Terms I and II often deviate from each other considerably at $y^+ = 12$, and even more so at $y^+ = 5$, as the instantaneous sum of terms III-VI (solid lines, red online), which degrade Taylor's hypothesis becomes large, indicating that the hypothesis has become a poor approximation very near the wall. Evident too, at all four y^+ locations, is that the phase agreement between the two Taylor's hypothesis terms I and II is rather good, even close to the wall, as was previously noted from the correlation coefficient plot in Fig. 8. The failure of Taylor's hypothesis near the wall is largely due to the amplitude differences between terms I and II.

The plots on the right-hand-side of the figure visually illustrate how each of the individual terms III-VI contribute to their net effect given by their sum. Note the change in vertical scale for these right-hand-side plots showing that these terms that diminish the validity of the Taylor's hypothesis approximation have much smaller amplitudes at the channel centerline than they have near the wall. Lines of data for the terms from Eq. (13) applied to the wall normal and spanwise velocity components and for the lower Reynolds number case, at the same y^+ locations, are very similar to those for the streamwise velocity component shown here.

B. Vorticity

Just as we did for the momentum transport, Eq. (6) describing the transport of vorticity can be rearranged as

$$\frac{\partial \omega_i}{\partial x}\Big|_I = \frac{1}{U_{c\omega_i}}[\underbrace{-\frac{\partial \omega_i}{\partial t}}_{II} + \underbrace{(\overline{\Omega}_j + \omega_j)\frac{\partial(\overline{U}_i + u_i)}{\partial x_j}}_{III} + \underbrace{\nu\frac{\partial^2(\overline{\Omega}_i + \omega_i)}{\partial x_j \partial x_j}}_{IV} - \underbrace{u_j\frac{\partial(\overline{\Omega}_i + \omega_i)}{\partial x_j}}_{V} + \underbrace{f_{\omega_i}(y^+)\frac{\partial \omega_i}{\partial x}}_{VI}],$$

(14)

where

$$f_{\omega_i}(y^+) = U_{c\omega_i} - \overline{U}$$

(15)

is obtained from the data in Fig. 5. Analogous to Eq. (11), if the terms on the right-hand-side of Eq. (14) following term II, namely, the stretching/compression/reorientation term III, the viscous diffusion term IV, and the additional convective rate of change term V, are each instantaneously very small or their sum is very small compared to the magnitude of the local rate of change term II (the first term on the right-hand-side of the equation), then Taylor's hypothesis, applied to the fluctuating vorticity field, is quite well satisfied in the region of the flow where the convection velocity is nearly equal to the mean velocity. As for the velocity field, this latter condition is approximately the case for $y^+ > 20$, but nearer the wall, the difference between the convection velocity and the mean velocity, expressed as the function $f_{\omega_i}(y^+)$, must also be accounted for, and this accounting is provided by term VI.

All the terms in Eq. (14) have zero mean values except for terms III, IV, and V, so, when the equation is averaged, it becomes

$$\overline{\omega_j\frac{\partial u_i}{\partial x_j}} + \nu\frac{\partial^2 \overline{\Omega}_i}{\partial x_j \partial x_j} - \overline{u_j\frac{\partial \omega_i}{\partial x_j}} = 0.$$

(16)

The first of the terms in Eq. (16) is the mean of term III in Eq. (14), and it represents the average rate of change of the vorticity fluctuations due to stretching/compression directly or through reorientation by the spatial gradients of the fluctuating velocity components. It can be alternatively expressed as the wall normal gradient of the vorticity-velocity covariance, $\partial\overline{\omega_y u_i}/\partial y$. The second term in Eq. (16) is the average of term IV in Eq. (14), $\nu\partial^2\overline{\Omega}_z/\partial y^2$, and it represents the viscous diffusion of the average vorticity. The third term in Eq. (16) is the mean of the additional convective rate of change of vorticity term V in Eq. (14). It can also be expressed as the wall normal gradient of the velocity-vorticity covariance, $\partial\overline{v\omega_i}/\partial y$. These mean terms only appear in the component form of Eq. (14) for the spanwise vorticity, and there they sum to zero. So, as for the velocity field, they have no net effect on the validity of Taylor's hypothesis applied to the vorticity field. This is demonstrated in Fig. 13 where the mean values of the terms in Eq. (14) are shown for each of the component equations for the vorticity fluctuations.

When Eq. (16) is subtracted from Eq. (14), the remainder is

$$\frac{\partial \omega_i}{\partial x}\Big|_I = \frac{1}{U_{c\omega_i}}\{\underbrace{-\frac{\partial \omega_i}{\partial t}}_{II} + \underbrace{[(\overline{\Omega}_j + \omega_j)\frac{\partial(\overline{U}_i + u_i)}{\partial x_j} - \overline{\omega_j\frac{\partial u_i}{\partial x_j}}]}_{III} + \underbrace{\nu\frac{\partial^2 \omega_i}{\partial x_j \partial x_j}}_{IV} -$$
$$\underbrace{[u_j\frac{\partial(\overline{\Omega}_i + \omega_i)}{\partial x_j} - \overline{u_j\frac{\partial \omega_i}{\partial x_j}}]}_{V} + \underbrace{f_{\omega_i}(y^+)\frac{\partial \omega_i}{\partial x}}_{VI}\}.$$

(17)

The streamwise spatial and temporal vorticity fluctuation derivative terms on either side of the equal sign (I and II) in Eq. (17) are clearly those in Taylor's hypothesis. They are expressed using the
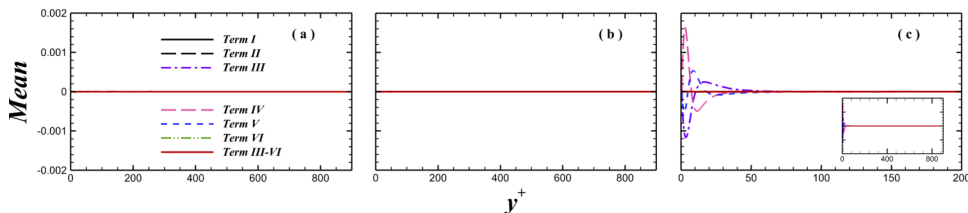

FIG. 13. Distributions of the mean values, normalized with ν/u_τ^2, of individual terms III-V and their sum from Eq. (16) for the (a) streamwise, (b) wall normal, and (c) spanwise vorticity components, all with the same vertical scale. Lines: long-short dashes (purple online), III; long dashes (red online), IV; short dashes (blue online), V; solid (scarlet online), sum of terms III-V. All the other terms that have zero mean values for all y^+ values are hidden in these plots by these sum of terms III-VI curves in the three plots.

optimized values of the convection velocities, $1/U_{c\omega_i}$, obtained with Eq. (7), where ω_i has been substituted for u_i, and that include all scales and depend on y^+. Thus, to reiterate, the hypothesis will be instantaneously quite well satisfied if each of the additional terms on the right-hand-side (III-VI) are instantaneously and individually quite small, compared to term II, or if they combine so that their sum is instantaneously quite small, compared to term II.

1. Average amplitudes of terms in Eq. (17)

As for the momentum transport analysis with Eq. (13), the average amplitudes of the terms in Eq. (17) are determined best with their rms values. The distributions of these rms values of the two Taylor's hypothesis terms, I and II, the individual terms III-VI, and the sum of terms III-VI from each of the three component equations of (17) for the vorticity fluctuations are plotted in Figs. 14(a)–14(c). Note again that the instantaneous values of the sum of terms III-VI include the instantaneous signs of the terms in the sum, so cancelation between terms can occur. Thus, the rms of this instantaneous sum of terms III-VI is a measure of the average amplitude of the combination of terms that diminish the validity of Taylor's hypothesis when it is applied to the vorticity field, just as for the velocity field using Eq. (13). The inset in the figure magnifies the values of the distributions for $y^+ < 10$.
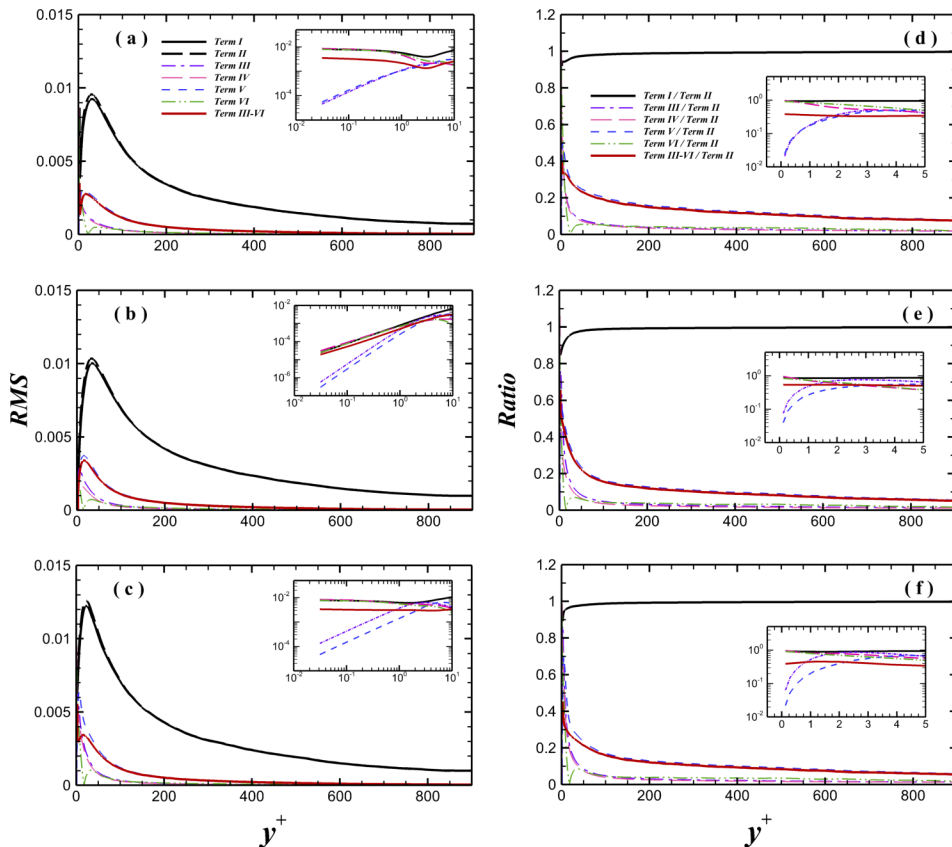

FIG. 14. Distributions of rms values, normalized with ν/u_τ^2, of individual terms I-VI and the sum of terms III-VI from Eq. (17) for the vorticity fluctuations: (a) streamwise, (b) wall normal, and (c) spanwise. Lines: upper solid (black online), I; upper long dashes (black online), II; long-short dashes (purple online), III; lower long dashes (red online), IV; short dashes (blue online), V; dashed-dotted-dotted-dashed (green online), VI; lower solid (scarlet online), sum of III-VI. Distributions of the ratios of the rms values of terms I, III-VI, and the sum of terms III-VI to the rms values of term II from Eq. (17) for the vorticity fluctuations: (d) streamwise, (e) wall normal, and (f) spanwise. Lines: upper solid (black online), I/II; long-short dashes (purple online), III/II; long dashes (red online), IV/II; short dashes (blue online), V/II; dashed-dotted-dotted-dashed (green online), VI/II; lower solid (scarlet online), sum of (III-VI)/II.

The relative magnitudes of the rms values of the terms in the component forms of Eq. (17) for vorticity fluctuations are shown in Figs. 14(d)–14(f), where the distributions are plotted of the ratios of the rms values of the convective rate of change term I, the individual terms III-VI, and the sum of terms III-VI to the rms values of the local rate of change of vorticity term II. Similar to the velocity field results, for $y^+ > 50$, the average amplitude of the ratio of the sum of terms III-VI to term II is a little more than 20% of the ratio of term I to term II for the streamwise component and less than 20% for the wall normal and spanwise components of the vorticity fluctuations, and this percentage diminishes even more further toward the channel centerline. In the viscous sublayer, the average amplitude of the ratio of the sum of terms III-VI to term II is about 35% of the ratio of term I to term II for the streamwise component equation and about 45% or greater for the wall normal and spanwise component equations. Terms IV and VI representing, respectively, viscous diffusion of vorticity and the effect of the differences between the convection velocities and the mean velocity, become particularly large relative to terms I and II in the viscous sublayer. This is clearly shown in all the insets of Fig. 14, indicating that, in this region, Taylor's hypothesis, applied to the vorticity field, is a quite poor approximation.

2. Probability density functions of the ratios of terms in Eq. (17)

As for the momentum equation analysis in Sec. V A, it is of interest to know how the probabilities of the instantaneous values of the amplitudes of the terms in Eq. (17) are distributed. In Figs. 15(a)–15(l), the PDFs are shown for the ratios, defined by term I, the individual terms III-VI, and the sum of terms III-VI, with each divided by term II, obtained from this transport equation for the
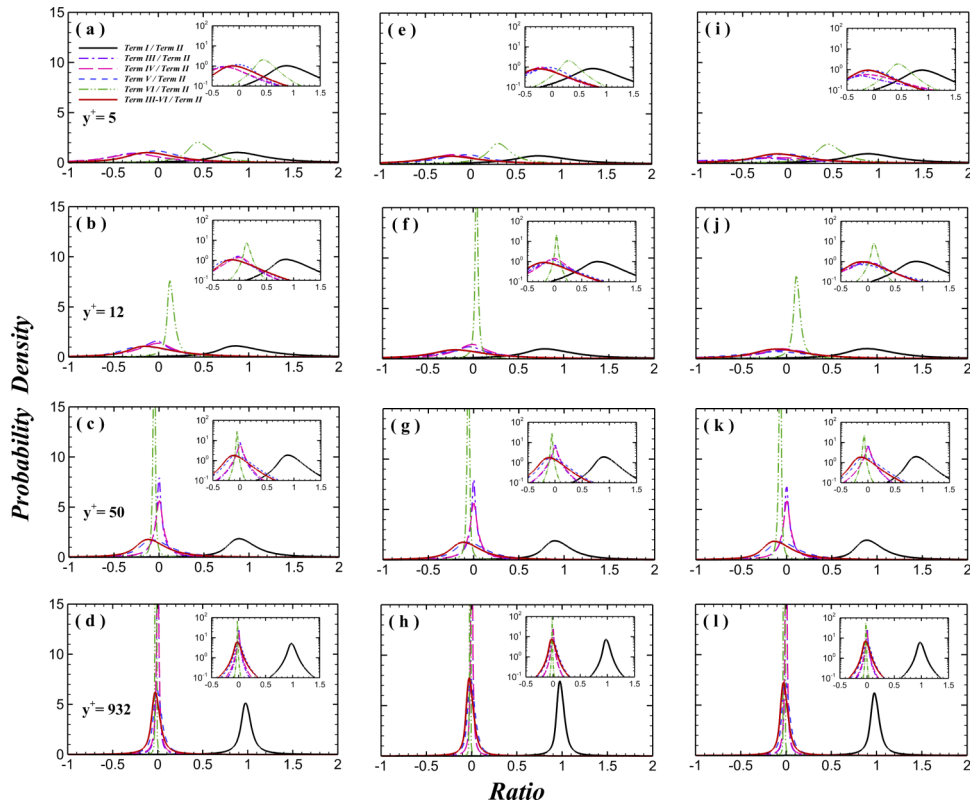

FIG. 15. PDFs of the ratios of terms I, III-VI, and the sum of III-VI to term II of Eq. (17) applied to the three vorticity components. From left to right: (a)-(d) streamwise vorticity, (e)-(h) wall normal vorticity, and (i)-(l) spanwise vorticity, and from top to bottom, $y^+ = 5$, $y^+ = 12$, $y^+ = 50$, and the channel centerline, $y^+ = 932$. Lines: right solid (black online), I/II; long-short dashes (purple online), III/II; long dashes (red online), IV/II; short dashes (blue online), V/II; dashed-dotted-dotted-dashed (green online), VI/II; left solid (scarlet online), sum of (III-VI)/II.
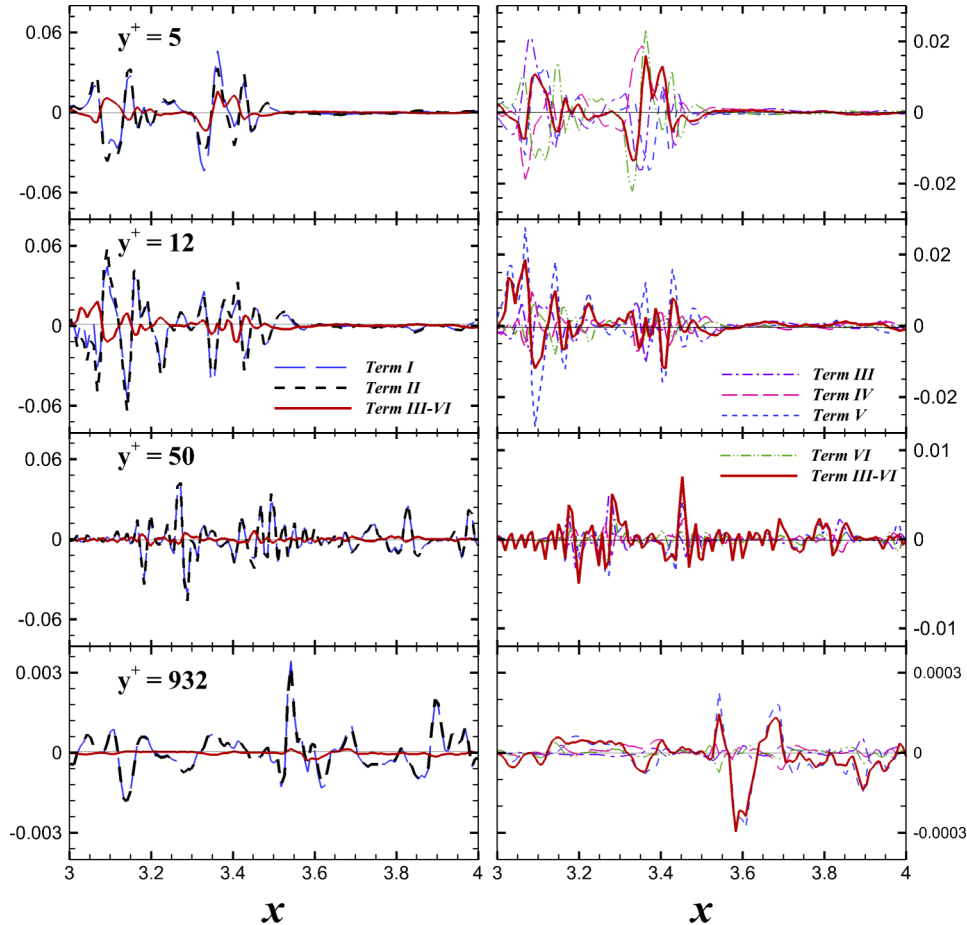
FIG. 16. Distributions of lines instantaneous values of lines of data in the x-direction from terms in Eq. (17) for the streamwise vorticity component at $y^+ = 5$, 12, 50, and the channel centerline. Lines left-side: long dashes (blue online), I; short dashes (black online), II; solid (scarlet online), sum of III-VI. Lines right-side: solid (scarlet online), sum of III-VI; long-short dashes (purple online), III; dashes (red online), IV; short dashes (blue online), V; dashed-dotted-dotted-dashed (green online), VI. Note the change in vertical scale of plots on the right-hand-side of this figure and for the lower plot on the left-hand-side.

vorticity components at $y^+ = 5$, 12, 50, and 932 (the channel centerline). The trends of the PDFs for the vorticity field are very similar to those for the velocity field. At the centerline, all the PDFs of these ratios are narrow compared to those near the wall for all three component equations. The PDFs of the ratio of the Taylor's hypothesis terms, I/II, have peak values near unity, whereas the peak values of the PDFs of the ratios of the other terms, compared to term II, are near zero. Just as for the velocity field, these observations make it clear that Taylor's hypothesis, applied to the vorticity field, is a reasonably good approximation at and near the channel centerline, although there is some significant probability of the instantaneous gradients $1/U_{c\omega_i}\partial\omega_i/\partial t$ and $\partial\omega_i/\partial x$ not being equal because of the significant probability that the ratio of the sum of terms III-VI to term II from these component equations is not small. Near the wall at $y^+ = 5$ and 12, the PDFs of all the terms are much broader. It is clear that the probability is much higher that the ratios of the Taylor's hypothesis terms, I/II, may be significantly different from unity in this high mean shear region. The PDFs at $y^+ = 50$ reflect the intermediate state between the channel centerline and the very near wall region.

The PDFs at these four locations in the flow for all three component equations also show how the values of the ratios of the individual terms III-VI to term II are distributed with respect to the distribution of the PDFs of the ratio of the sum of their instantaneous values to term II. Noteworthy is that the PDFs of the ratios of term VI, accounting for the difference between the convection velocities and the mean velocity, to term II have different comportments than the other ratios of the terms,

III-V, to term II, just as for the velocity field. The PDFs of VI/II ratios are narrower, and their most probable values move toward the most probable values of the ratios I/II as the wall is approached, indicating the diminishment of the validity of Taylor's hypothesis caused by term VI. Noteworthy also is that the PDFs of the ratios of terms III and IV to term II, i.e., the terms that account for stretching/compression/reorientation and viscous diffusion of the vorticity components, respectively, are very broad at the edge of the viscous sublayer at $y^+ = 5$ with most probable values that are negative and significantly different from zero.

3. Instantaneous x-direction distributions of the terms in Eq. (17)

As for the momentum transport analysis, lines of instantaneous data in the x-direction along the center of the homogeneous planes at $y^+ = 5, 12, 50$, and the channel centerline, for the terms in Eq. (17) applied to the streamwise vorticity component, are plotted in Fig. 16 to help us visualize how these terms affect the instantaneous validity of Taylor's hypothesis. Observations made in Sec. V A 3 about Fig. 12 for the velocity field instantaneous line of data, are equally applicable here for the vorticity field data.

VI. SUMMARY AND CONCLUSIONS

1. Taylor's "frozen turbulence" hypothesis states that the streamwise spatial gradients of the velocity fluctuations, $\partial u_i/\partial x$, can be well approximated by the products of inverse convection velocities and the time derivatives of the velocity fluctuations, $1/U_{c u_i}(\partial u_i/\partial t)$, under suitable conditions. This time-space transformation can be applied to any flow property, the evolution of which is described by a transport equation. Here, the hypothesis has been examined for velocity *and* vorticity fluctuations using a low Reynolds number turbulent channel flow DNS at $Re_\tau = 205$ and a higher Reynolds number DNS at $Re_\tau = 932$.

2. An expression was derived to determine the optimal convection velocities, $U_{c u_i}$ using the instantaneous values of $\partial u_i/\partial t$ and $\partial u_i/\partial x$, and it confirmed the expression previously obtained by del Álamo and Jiménez.[27] Substituting ω_i for u_i, the same expression was used to determine the optimal convection velocities, $U_{c \omega_i}$ for the fluctuations of the vorticity field.

3. These convection velocities for the velocity and vorticity component fluctuations were compared to those found by Kim and Hussain[23] from space-time correlations in a channel flow DNS at a similar Reynolds number as our lower one. The agreement is excellent. As they found, for $y^+ > 20$, the convection velocities for each of the velocity and vorticity components are close to each other and to the local mean velocity. Below this location, the convection velocities are increasingly larger than the local mean velocity as the wall is approached. For $y^+ < 5$, in the viscous sublayer, the convection velocities are very nearly constant with values of between $9u_\tau$ and $10u_\tau$ for the velocity field, and between $8u_\tau$ and $10u_\tau$ for the vorticity field.

4. At the channel centerline, joint PDFs show that most of the $U_{c u}\partial u/\partial x$ and $-\partial u/\partial t$ and the $U_{c \omega_x}\partial \omega_x/\partial x$ and $-\partial \omega_x/\partial t$ data pair ratios fall within a region defined by 1 ± 0.2. As the wall is approached, much of these data falls outside of this region.

5. Correlation coefficients for $U_{c u_i}\partial u_i/\partial x$ and $-\partial u_i/\partial t$ as well as for $U_{c \omega_i}\partial \omega_i/\partial x$ and $-\partial \omega_i/\partial t$, calculated from our DNSs, are greater than 0.85 for all three velocity and vorticity fluctuation components throughout the channel and are even greater than about 0.96 for $y^+ > 30$. This indicates a very high average phase agreement between these space and time derivatives, a fact visually confirmed in plots of instantaneous lines of data for these Taylor's hypothesis terms. These results also agree rather well with the LES results for the velocity field of Piomelli *et al.*[22] except in the buffer layer where the lack of resolution of the small scales by the LES and the use of subgrid scale modeling in their study is evident.

6. The mean values of the terms in the momentum transport equation, given by Eq. (11), are all zero or very small except for the pressure gradient term (III) and the viscous stress term (IV), and the fluctuating convective acceleration term (V). Although all three of these terms are always instantaneously present, they offset each other so that they have no net effect on the validity of Taylor's

hypothesis. This is also the case for mean values of the terms in the vorticity transport equation, given by Eq. (14), which are also all zero except for the stretching/compression/reorientation term (III), the viscous diffusion term (IV), and the fluctuating convective rate of change term (V). As for the momentum equation, although all three of these terms are always instantaneously present, they offset each other so that they also have no net effect on the validity of Taylor's hypothesis.

7. The average amplitudes of the temporal and streamwise derivative terms that comprise Taylor's hypothesis and that appear in both the momentum and vorticity transport equations for each component direction, as measured by their rms values, are considerably larger than the rest of the terms in those equations that act to diminish the validity of the hypothesis, except near the wall. For $y^+ > 50$, average amplitudes of the sums of the terms that diminish the validity of Taylor's hypothesis [terms III-VI in each of Eqs. (13) and (17)] are only a little greater than 20% for the streamwise component and less than 20% for the wall normal and spanwise components of the terms that make up the hypothesis, and this percentage diminishes even more further toward the channel centerline. On the other hand, in the viscous sublayer, these average amplitudes rise to more than 50% of the terms making up Taylor's hypothesis for the streamwise velocity component.

8. PDFs of the ratios of instantaneous values of all the other terms in the momentum transport Eq. (13) for the velocity components, compared to local acceleration term II, $1/U_{c u_i}(\partial u_i/\partial t)$, show how the range of variability of these terms increases going from the channel centerline to the viscous sublayer. At the centerline, for all three component equations, the PDFs are narrow, with the most probable values of ratios of the temporal and streamwise derivative terms comprising Taylor's hypothesis near unity, whereas the most probable values of the ratios, compared to term II, of the sum of the other terms (III-VI) that diminish the validity of Taylor's hypothesis are near zero, indicating that Taylor's hypothesis is a good approximation. Near the wall for $y^+ < 50$, the PDFs of these ratios are much broader and overlapping with most probable values not near unity and zero for the I/II and the sum of III-VI/II terms, respectively, indicating the much diminished validity of Taylor's hypothesis. The comportment of the PDFs for the vorticity components are quite similar, so similar conclusions can be drawn. It is worth pointing out, however, that this similarity of comportment of these and other plots for the vorticity field, compared to those for the velocity field, is not *a priori* self-evident. The physical mechanisms that diminish the validity of Taylor's hypothesis, described by the "non-Taylor's hypothesis" terms in the momentum and vorticity transport equations, respectively, are very different for the two equations. Thus, this similarity of comportment is itself significant.

9. Examples of lines of these momentum and vorticity transport instantaneous terms from Eqs. (13) and (17), for the streamwise direction and along the centerlines of the homogeneous planes at $y^+ = 5, 12, 50,$ and 932, vividly illustrate that the two Taylor's hypothesis terms, with the optimal convection velocity, are in very good agreement at the channel centerline and even reasonably so at $y^+ = 50$. However, this agreement becomes quite poor as the wall is approached, especially in the viscous sublayer. Noteworthy, though, is that this lack of agreement near the wall between the streamwise spatial derivatives and the temporal derivatives in Taylor's hypothesis is largely due to instantaneous differences in the amplitudes of these terms. The terms display good phase agreement, even very near the wall, as was also indicated by their correlation coefficients.

[1] G. I. Taylor, "Production and dissipation of vorticity in a turbulent fluid," Proc. R. Soc. A **164**, 15 (1938).

[2] G. I. Taylor, "The spectrum of turbulence," Proc. R. Soc. A **164**, 476 (1938).

[3] C. C. Lin, "On Taylor's hypothesis and the acceleration terms in the Navier-Stokes equations," Q. Appl. Math. **10**, 295 (1953).

[4] M. J. Fisher and P. O. A. L. Davies, "Correlation measurements in a non-frozen pattern of turbulence," J. Fluid Mech. **18**, 97 (1964).

[5] J. L. Lumley, "Interpretation of time spectra measured in high-intensity shear flows," Phys. Fluids **8**, 1056 (1965).

[6] R. J. Hill, "Corrections to Taylor's frozen turbulence approximation," Atmos. Res. **40**, 153 (1996).

[7] E. Gledzer, "On Taylor's hypothesis corrections for measured energy spectra of turbulence," Phys. D **104**, 163 (1997).

[8] G. Hekestad, "A generalized Taylor hypothesis with application for high Reynolds number turbulent shear flows," J. Appl. Mech. **32**, 735 (1965).

[9] H. Tennekes, "Eulerian and Lagrangian time microscales in isotropic turbulence," J. Fluid Mech. **67**, 561 (1975).

[10] M. Pinsky, A. Khain, and A. Tsinober, "Accelerations in isotropic and homogeneous turbulence and Taylor's hypothesis," Phys. Fluids **12**, 3195 (2000).

[11] R. B. Loucks and J. M. Wallace, "Velocity and velocity gradient based properties of a turbulent plane mixing layer," J. Fluid Mech. **699**, 213 (2012).

[12] K. B. M. Q. Zaman and A. K. M. F. Hussain, "Taylor hypothesis and large-scale coherent structures," J. Fluid Mech. **112**, 379 (1981).

[13] L. W. B. Browne, R. A. Antonia, and S. Rajagopalan, "The spatial derivative of temperature in turbulent flow and Taylor's hypothesis," Phys. Fluids **26**, 1222 (1983).

[14] A. Cendese, G. P. Romano, and F. D. Felice, "Experimental testing of Taylor's hypothesis by L.D.A. in highly turbulent flow," Exp. Fluids **11**, 351 (1991).

[15] G. P. Romano, "Analysis of two-point velocity measurements in near-wall flows," Exp. Fluids **20**, 68 (1991).

[16] W. J. A. Dahm and K. B. Southerland, "Experimental assessment of Taylor's hypothesis and its application to dissipation estimates in turbulent flows," Phys. Fluids **9**, 2101 (1997).

[17] V. S. L'vov, A. Pomyalov, and I. Procaccia, "Temporal surrogates of spatial turbulent statistics: The Taylor hypothesis revisited," Phys. Rev. E **60**, 4175 (1999).

[18] B. Ganapathisubramani, K. Lakshminarasimhan, and N. T. Clemens, "Determination of complete velocity gradient tensor by using cinematographic stereoscopic PIV in a turbulent jet," Exp. Fluids **42**, 923 (2007).

[19] N. Hutchins and I. Marusic, "Evidence of very long meandering features in the logarithmic region of the turbulent boundary layers," J. Fluid Mech. **579**, 1 (2007).

[20] D. J. C. Dennis and T. B. Nickels, "On the limitations of Taylor's hypothesis in constructing long structures in a turbulent boundary layer," J. Fluid Mech. **614**, 197 (2008).

[21] S. Davoust and L. Jacquin, "Taylor's hypothesis convection velocities from mass conservation equation," Phys. Fluids **23**, 051701 (2011).

[22] U. Piomelli, J.-L. Balint, and J. M. Wallace, "On the validity of Taylor's hypothesis for wall-bounded turbulent flows," Phys. Fluids A **1**, 609 (1989).

[23] J. Kim and F. Hussain, "Propagation velocity of perturbations in turbulent channel flow," Phys. Fluids A **5**, 695 (1993).

[24] S. Lee, S. K. Lele, and P. Moin, "Simulation of spatially evolving turbulence and the applicability of Taylor's hypothesis in compressible flow," Phys. Fluids A **4**, 1521 (1992).

[25] A. Tsinober, P. Vedula, and P. K. Yeung, "Random Taylor hypothesis and the behavior of local and convective accelerations in isotropic turbulence," Phys. Fluids **13**, 1974 (2001).

[26] S. Tardu and P. Vezin, "On the Taylor hypothesis in forced unsteady wall flows," Exp. Fluids **39**, 909 (2005).

[27] J. C. del Alámo and J. Jiménez, "Estimation of turbulent convection velocities and corrections to Taylor's approximation," J. Fluid Mech. **640**, 5 (2009).

[28] P. Moin, "Focus on fluids: Revisiting Taylor's hypothesis," J. Fluid Mech. **640**, 1 (2009).

[29] G.-W. He and J. B. Zhang, "Elliptic model for space–time correlations in turbulent shear flows," Phys. Rev. E **73**, 055303 (2006).

[30] X. Zhao and G.-W. He, "Space–time correlations of fluctuating velocities in turbulent shear flows," Phys. Rev. E **164**, 046316 (2009).

[31] J. A. Wills, "On convection velocities in turbulent shear flows," J. Fluid Mech. **20**, 417 (1964).

[32] X. He, G.-W. He, and P. Tong, "Small-scale turbulent fluctuations beyond Taylor's frozen-flow hypothesis," Phys. Rev. E. **81**, 065303 (2010).

[33] Q. Zhou, C. M. Li, Z. M. Lu, and Y. L. Liu, "Experimental investigation of longitudinal space-time correlations of the velocity field in turbulent Rayleigh-Benard convection," J. Fluid Mech. **683**, 94 (2011).

[34] J. Hogg and G. Ahlers, "Reynolds-number measurements for low-Prandtl-number turbulent convection of large-aspect ratio samples," J. Fluid Mech. **725**, 664 (2013).

[35] A. Lozano-Durán and J. Jiménez, "Effect of the computational domain on direct simulations of turbulent channels up to R_τ = 4200," Phys. Fluids **26**, 011702 (2014).

[36] J. Kim, P. Moin, and R. Moser, "Turbulence statistics in fully developed channel flow at low Reynolds number," J. Fluid Mech. **177**, 133 (1987).

[37] G. E. Karniadakis, M. Israeli, and S. A. Orszag, "High-order splitting methods for the incompressible Navier–Stokes equations," J. Comput. Phys. **97**, 414 (1991).

[38] P. R. Spalart, R. D. Moser, and M. M. Rogers, "Spectral methods for the Navier-Stokes equations with one infinite and two periodic directions," J. Comput. Phys. **96**, 297 (1991).

[39] J. Jiménez and P. Moin, "The minimal flow unit in near-wall turbulence," J. Fluid Mech. **225**, 280 (1991).

[40] J. Jiménez, "Transition to turbulence in two dimensional Poiseuille flow," J. Fluid Mech. **218**, 265 (1990).

[41] P. V. Vukoslavčević, N. Beratlis, E. Balaras, J. M. Wallace, and O. Sun, "On the spatial resolution of velocity and velocity gradient-based turbulence statistics measured with multi-sensor hot-wire probes," Exp. Fluids **46**, 109 (2009).